New Phytologist

A mis-regulated cyclic nucleotide-gated channel mediates cytosolic calcium elevation and activates immunity in Arabidopsis

Chunhui Zhao[1]*, Yinhua Tang[1]*, Junli Wang[2], Yanhong Zeng[1], Hequan Sun[3], Zichao Zheng[1], Rong Su[1], Korbinian Schneeberger[3], Jane E. Parker[2,4] and Haitao Cui[1]

[1]Key Laboratory of Ministry of Education for Genetics, Breeding and Multiple Utilization of Crops, Fujian University Key Laboratory for Plant–Microbe Interaction, Plant Immunity Center, Fujian Agriculture and Forestry University, Fuzhou 350002, China; [2]Department of Plant-Microbe Interactions, Max-Planck Institute for Plant Breeding Research, Carl-von-Linné Weg 10, Cologne 50829, Germany; [3]Department of Chromosome Biology, Max-Planck Institute for Plant Breeding Research, Carl-von-Linné Weg 10, Cologne 50829, Germany; [4]Cologne-Duesseldorf Cluster of Excellence on Plant Sciences (CEPLAS), Duesseldorf 40225, Germany

Authors for correspondence:
Haitao Cui
Email: cui@fafu.edu.cn

Jane E. Parker
Email: parker@mpipz.mpg.de

Received: *31 March 2020*
Accepted: *9 January 2021*

New Phytologist (2021) **230:** 1078–1094
doi: 10.1111/nph.17218

Key words: calcium channel, CNGC, EDS1 (ENHANCED DISEASE SUSCEPTIBLITY1), ETI (effector-triggered immunity), plant immunity, PTI.

Summary

- Calcium (Ca^{2+}) is a second messenger for plant cell surface and intracellular receptors mediating pattern-triggered and effector-triggered immunity (respectively, PTI and ETI). Several CYCLIC NUCLEOTIDE-GATED CHANNELS (CNGCs) were shown to control transient cytosolic Ca^{2+} influx upon PTI activation. The contributions of specific CNGC members to PTI and ETI remain unclear.
- ENHANCED DISEASE SUSCEPTIBLITY1 (EDS1) regulates ETI signaling. In an Arabidopsis genetic screen for suppressors of *eds1*, we identify a recessive gain-of-function mutation in *CNGC20*, denoted *cngc20-4*, which partially restores disease resistance in *eds1*.
- *cngc20-4* enhances PTI responses and ETI hypersensitive cell death. *A cngc20-4* single mutant exhibits autoimmunity, which is dependent on genetically parallel *EDS1* and salicylic acid (SA) pathways. CNGC20 self-associates, forms heteromeric complexes with CNGC19, and is phosphorylated and stabilized by BOTRYTIS INDUCED KINASE1 (BIK1). The *cngc20-4* L371F exchange on a predicted transmembrane channel inward surface does not disrupt these interactions but leads to increased cytosolic Ca^{2+} accumulation, consistent with mis-regulation of CNGC20 Ca^{2+}-permeable channel activity.
- Our data show that ectopic Ca^{2+} influx caused by a mutant form of CNGC20 in *cngc20-4* affects both PTI and ETI responses. We conclude that tight control of the CNGC20 Ca^{2+} ion channel is important for regulated immunity.

Introduction

Plants have two immune receptor systems for recognizing invading microbes and activating defenses that limit infection (Jones & Dangl, 2006). The first is governed by plasma membrane-localized pattern recognition receptors (PRRs), which perceive pathogen/microbe associated molecular patterns (PAMPs/MAMPs) or damage associated molecular patterns (DAMPs) to activate pattern-triggered immunity (PTI). The second, effector-triggered immunity (ETI), is mostly controlled by intracellular nucleotide-binding leucine-rich-repeat (NLR) receptors, which are activated by pathogen effectors (virulence factors) to accelerate and amplify defenses (Cui *et al.*, 2015; Kadota *et al.*, 2019; Wang *et al.*, 2020). Effector-triggered immunity often culminates in host localized cell death (a hypersensitive response, HR). Pattern-triggered immunity and ETI mobilize qualitatively similar outputs, including transient calcium (Ca^{2+}) influx to the cytosol, production of reactive oxygen species (ROS) and nitric oxide, induced MITOGEN-ACTIVATED PROTEIN KINASE (MAPK) cascades and transcriptional defense reprogramming (Cui *et al.*, 2015; Liang & Zhou, 2018). If prolonged, these defenses lead to plant growth inhibition and lesioning.

Two major NLR receptor types are characterized by their distinctive N-terminal signaling domains: a coiled-coil domain in CC-NLRs (CNLs) and a Toll-Interleukin1-Receptor (TIR) domain in TIR-NLRs (TNLs) (Jubic *et al.*, 2019). How NLR receptors connect molecularly to defense and cell death execution pathways is not resolved, although several signaling NLR families and the early transducer ENHANCED DISEASE SUSCEPTIBILITY1 (EDS1) control ETI cell death and pathogen resistance (Cui *et al.*, 2015; Lapin *et al.*, 2019, 2020). Arabidopsis EDS1 forms heterodimers with its sequence-related partners PHYTOALEXIN DEFICIENT4 (PAD4) and SENESCENCE ASSOCIATED GENE101 (SAG101) for signaling in TNL ETI (Feys *et al.*, 2001, 2005; Wagner *et al.*, 2013; Bhandari *et al.*, 2019; Lapin *et al.*, 2019). The EDS1-PAD4

*These authors contributed equally to this work and are first co-authors.

heterodimer has a basal immunity activity which limits growth of virulent pathogens (Rietz *et al.*, 2011; Cui *et al.*, 2017; Lapin *et al.*, 2020). Arabidopsis EDS1-PAD4 promoted basal and ETI defenses involve transcriptional boosting of the biotic stress hormone salicylic acid (SA) pathway and dampening of jasmonic acid hormone signaling, which contributes to pathogen growth restriction (Bartsch *et al.*, 2006; Fu & Dong, 2013; Cui *et al.*, 2017, 2018; Bhandari *et al.*, 2019).

Recent insights into molecular activation mechanisms for TNL and CNL receptors suggest that they lead to ETI host cell death responses in different ways. Self-associating TIR domains of several TNLs have an NAD^+ase enzymatic activity linked to *EDS1*-dependent plant cell death (Horsefield *et al.*, 2019; Wan *et al.*, 2019). Protein structural studies have revealed that NAD^+ hydrolase activity of TNL receptors RECOGNITION OF PERONOSPORA PARASITICA1 (RPP1) and RECOGNITON OF XOPQ1 (ROQ1) is activated by pathogen effector-induced assembly of a tetrameric 'resistosome' complex (Ma *et al.*, 2020; Martin *et al.*, 2020). TNL-triggered cell death is conferred by the EDS1-SAG101 heterodimer, together with the N REQUIRED GENE1 (NRG1) sub-family of signaling NLRs (Qi *et al.*, 2018; Gantner *et al.*, 2019; Lapin *et al.*, 2019). By contrast, the Arabidopsis effector-activated CNL receptor HOPZ-ACTIVATED RESISTANCE1 (ZAR1) assembles into a pentameric complex to form a potential plasma membrane-associated ion channel or pore (Wang *et al.*, 2019a, c), which might represent autonomous cell death-triggering capacity of CNL receptors (Jubic *et al.*, 2019; Wang *et al.*, 2019a).

Calcium is a secondary messenger for numerous signaling pathways in eukaryotic cells. In plants, regulated Ca^{2+} influx is necessary for HR cell death in ETI (Atkinson *et al.*, 1990; Grant *et al.*, 2000; Moeder *et al.*, 2019). Also, a Ca^{2+} burst leading to transient cytosolic Ca^{2+}elevation is a critical early step in PTI signaling (Blume *et al.*, 2000; Ranf *et al.*, 2011; Ma *et al.*, 2012, 2013). Ca^{2+} influx occurs upstream of CALCIUM-DEPENDENT PROTEIN KINASES (CPKs) which promote an ROS burst, and Ca^{2+} blockers reduce MAPK activation by PAMPs (Grant *et al.*, 2000; Kobayashi *et al.*, 2007; Boudsocq *et al.*, 2010; Moeder *et al.*, 2019). Elevation of cytosolic Ca^{2+} upon PAMP/DAMP perception requires Ca^{2+} entry across the plasma membrane through Ca^{2+} channels (Seybold *et al.*, 2014; Moeder *et al.*, 2019). In Arabidopsis and rice, CYCLIC NUCLEOTIDE-GATED ION CHANNELS (CNGCs) were shown to contribute to plant immunity by increasing cytosolic Ca^{2+} (Moeder *et al.*, 2019; Wang *et al.*, 2019b). CNGC2 was discovered by characterization of an Arabidopsis null mutant '*defense, no death*' (*dnd1)* with reduced HR cell death in ETI (Clough *et al.*, 2000). The *dnd1* mutant has an autoimmune phenotype with constitutive *PATHOGENESIS-RELATED* (*PR*) gene expression and high SA accumulation (Yu *et al.*, 1998; Clough *et al.*, 2000). A family of DAMP peptides (*At*Peps) which promote systemic immunity also induced CNGC2-dependent Ca^{2+} influx in Arabidopsis (Qi *et al.*, 2010). Moreover, CNGC2 controlled Ca^{2+} channel activity and Ca^{2+} unloading from the vasculature into leaf cells (Wang *et al.*, 2017). A similar 'defense, no death' phenotype to *dnd1* was observed in Arabidopsis *dnd2*, a *CNGC4* null mutant (Jurkowski *et al.*, 2004). The CNGC2 and CNGC4 proteins interact to form a functional Ca^{2+} channel which is blocked by bound calmodulin in its resting state (Tian *et al.*, 2019). In response to PAMP/DAMP perception by PRRs, the CNGC2/CNGC4 channel is phosphorylated and activated by cytoplasmic receptor-like kinase (RLCK) BOTRYTIS INDUCED KINASE1 (BIK1), leading to elevated cytosolic Ca^{2+} (Liang & Zhou, 2018; Tian *et al.*, 2019). Incomplete loss of the PAMP-triggered ROS burst and Ca^{2+} influxes in Arabidopsis *cngc2 cngc4* mutants suggested roles of further Ca^{2+} channels in PTI signaling (Tian *et al.*, 2019). Another CNGC, *At*CNGC19 acts as a Ca^{2+}-permeable inward channel which promotes defenses against an insect herbivore, *Spodoptera litura* (Meena *et al.*, 2019). BRI1-ASSOCIATED RECEPTOR KINASE1 (BAK1) and its closest homolog, SOMATIC-EMBRYOGENESIS RECEPTOR KINASE4 (SERK4), function as coreceptors of many PRRs in PTI and negatively regulate plant cell death (Gao *et al.*, 2018; Liang & Zhou, 2018). A function of CNGC20 and CNGC19 as a Ca^{2+}-permeable channel regulating cell death in *bak1/serk4* was recently reported (Yu *et al.*, 2019).

In a genetic screen for suppressors of Arabidopsis *eds1-2* disease susceptibility, we identify and characterize a recessive gain-of-function *CNGC20* mutant (*cngc20-4*) that exhibits autoimmunity. We provide evidence that *cngc20-4* leads to elevated Ca^{2+} cytosolic accumulation which enhances PTI and ETI. We further establish that BIK1 phosphorylates and stabilizes CNGC20. Our data suggest that a mis-regulated CNGC20 Ca^{2+} channel can promote both PTI and ETI anti-pathogen defenses and that *cngc20-4* might serve as a tool to understand convergence between these two immunity layers.

Materials and Methods

Plant materials, growth conditions and pathogen strains

Arabidopsis thaliana accession Col-0 (Col) was used in all experiments. The *eds1-2* (Bartsch *et al.*, 2006), *sid2-1* (Wildermuth *et al.*, 2001), *cngc20-1*, and *cngc19-1* (Kugler *et al.*, 2009) mutants have been described in previous studies. The *eds1-2 sped1* double mutant was isolated from an *eds1-2* suppressor screen (Cui *et al.*, 2018). A *cngc20-4* (*sped1*) single mutant was generated by crossing *eds1-2 sped1* with Col. *Cngc20-4 sid2-1* and *cngc20-4 eds1-2 sid2-1* mutants were generated by crossing *eds1-2 sped1* with *sid2-1*. *Pseudomonas syringe* pv *tomato* (*Pst*) strain DC3000 and *Pst AvrRps4* were maintained as described previously (Cui *et al.*, 2017). Plants were grown under a 9 h : 15 h, light : dark photoperiod (with a light intensity of 150 µmol m^{-2} s^{-1}) at 22°C and 65% relative humidity.

Golden Gate cloning and generation of Arabidopsis transgenic lines

A coding sequence of *CNGC20* without a stop codon was amplified from Arabidopsis Col cDNA and cloned into Level 0 vector

pAGM1287. The *CNGC20* coding sequence was then cloned into L2 vector pICH86966 to fuse it with a CaMV 35S constitutive promoter and C-terminal yellow fluorescent protein (YFP) tag (*p35S:CNGC20-YFP-35S_term*). The backbones (pAGM1287, pICH86966), 35S promoter (pICH51266) and terminator (pICH41414) modules are from the Golden Gate cloning toolkit (Addgene, Watertown, MA USA) (Engler *et al.*, 2014). Sequences of primers used for cloning are provided in Supporting Information Table S1. The *p35S:CNGC20-YFP-35S_term* construct was transformed into *Agrobacterium* GV3101, and transgenic lines were generated by *Agrobacterium*-mediated floral dipping of Arabidopsis *eds1-2 sped1* plants.

Whole-genome resequencing-based mapping of *sped1*

Fifty F2 individuals in the backcrossed progeny with enhanced resistance to *Pst* AvrRps4 were pooled for DNA extraction, library preparation and sequencing. Raw reads were aligned against the Col-0 reference genome (TAIR10) using GenomeMapper (Schneeberger *et al.*, 2009). Short-read alignments were corrected for read-pair information and base calling was performed with Shore (Ossowski *et al.*, 2008). With the resequencing data, the causal mutations underlying *eds1-2 sped1* were predicted by SHOREmap v.3.0 (http://shoremap.org) (Sun & Schneeberger, 2015).

Sequence alignment and phylogenetic analysis

Protein sequences for 20 CNGCs were downloaded from The Arabidopsis Information Resource (TAIR; http://www.arabidopsis.org). The sequences were aligned using Muscle (https://www.ebi.ac.uk/Tools/msa/muscle/). Phylogenetic trees were generated by the neighbor-joining algorithms in Mega7 software (https://www.megasoftware.net). Bootstrap values were calculated using 100 replicates.

Pathogen infection assays

For bacterial growth assays, *Pst* DC3000 or *Pst AvrRps4* were cultured in King's B (KB) medium at 28°C overnight. The bacterial culture was diluted in H_2O at $OD_{600} = 0.0002$ for hand infiltration into leaves of 4-wk-old plants. Bacterial titers at 3 d post inoculation (dpi) were measured as previously described (Feys *et al.*, 2005). Statistical analysis of bacterial growth data from six biological replicates (as indicated in the figure legends) was done by one-way ANOVA followed by Tukey's HSD.

RNA analysis

Total leaf RNA was extracted using TRIzol Regent (cat. no. 15596018; Invitrogen) according to instructions. Briefly, 1 µg total RNA was used for cDNA synthesis (cat. no. M1705; Promega). Real-time quantitative polymerase chain reaction (qRT-PCR) analysis was performed on a CFX Connect machine (Bio-Rad). Normalization of expression against *AT4G26410* was performed as described (Cui *et al.*, 2017). The primers used are listed in Table S1.

Ion leakage assays

Ion leakage assays on detached Arabidopsis leaves were performed as described by Heidrich *et al.* (2011). Ion leakage assays in *Nicotiana benthamiana* were performed as described by Lapin *et al.* (2019).

PAMP- and DAMP-induced growth inhibition assays

The flg22- or Pep1-induced growth inhibition assays were performed as described by Navarro *et al.* (2008). The length of seedling root was measured 7 d after PAMP treatment.

ROS measurements

Leaf discs of 0.25 cm^2 were excised from 5-wk-old plants, followed by an overnight incubation in a 96-well plate with 200 µl of H_2O. H_2O was replaced by 100 µl reaction solution (20 µM luminol, 1 µg ml^{-1} of horseradish peroxidase) supplemented with 500 nM flg22 or Pep1. Reactive oxygen species measurements were conducted immediately using a luminometer (GM2000; Promega) with a 1-min interval reading time over a period of 30 min.

MAPK assays

For MAPK activation assays, 1 µM flg22 peptide was infiltrated into leaves of 4-wk-old plants. Total protein samples were collected at 0, 5, 15, 30, 60 min and used for immunoblotting with anti-p44/42 MAPK antibody (cat. no. 4370; Cell Signaling Technology, Danvers, MA, USA) to detect activated forms of MPKs (Suarez-Rodriguez *et al.*, 2007).

Transient expression in Arabidopsis protoplasts

Protoplast preparations from 4-wk-old Arabidopsis plants and transfections were performed as described (Li *et al.*, 2014). After transfection, protoplasts were incubated at room temperature under weak light (1.5 µmol m^{-2} s^{-1}) for 16 h, and protein extracts were prepared for immunoblotting and IP assays.

Protein extraction, immunoprecipitation and immunoblotting

Total leaf proteins were processed in extraction buffer (50 mM Tris pH7.5, 150 mM NaCl, 10% (v/v) glycerol, 2 mM EDTA, 5 mM DTT, protease inhibitor (Roche, 1 tablet per 50 ml), 0.1% Triton). Lysates were centrifuged for 15 min at 20 000 ***g*** at 4°C. Aliquots of supernatants were taken as input samples. Immunoprecipitations (IPs) were conducted by incubating supernatants with 15 µl GFP-Trap beads (ChromoTek, Germany) in 1.5 ml tubes for 2 h at 4°C. Beads were collected by centrifugation at 1000 ***g*** and washed four times in extraction buffer. Beads

were then heated in 2× Laemmli loading buffer, and proteins were separated by sodium dodecyl sulfate-polyacrylamide gel electrophoresis (SDS-PAGE) and analyzed by immunoblotting. Antibodies used were anti-GFP (cat. no. HT801; Transgen) and anti-HA (cat. no. 11867423001; Roche).

In vitro phosphorylation assay

The *in vitro* phosphorylation assay was performed as described previously (Tian *et al.*, 2019). Briefly, glutathione S-transferase (GST)-fused CNGC20CT and GST-BIK1 expressed in *Escherichia coli* BL21 strain were purified with Pierce glutathione agarose (Thermo Fisher Scientific, Carlsbad, CA, USA) as described by Li *et al.* (2014). Approximately 0.2 µg of each protein was incubated in kinase reaction buffer containing 20 mM HEPES (pH 7.5, adjusted with NaOH), 10 mM $MgCl_2$, 1 mM $MnCl_2$, 1 mM DTT, and 10 µM ATP at 30°C for 20 min. Samples were then separated on a 10% SDS-PAGE gel, followed by immunoblotting with anti-phosphor-threonine (cat. no. 9386; Cell Signaling Technology) or anti-GST (cat. no. ab19256; Abcam, Cambridge, UK) antibodies.

Cell-free protein stability assay

CNGC20CT-FLAG was transiently expressed in Arabidopsis Col protoplasts and purified by immunoprecipitation (IP) on anti-FLAG agarose. Total plant protein was first extracted with extraction buffer (25 mM Tris-HCl, pH7.5, 10 mM NaCl, 10 mM $MgCl_2$, 10 mM ATP, 5 mM DTT) from 4-wk-old leaves. Protein concentration was determined by the Bradford assay and 200 µg total protein was mixed with anti-FLAG agarose bound with CNGC20CT-FLAG. The protein mixture was incubated at 30°C for 2, 15, or 30 min, and the reaction was stopped by adding 2× Laemmli/SDS sample buffer.

Bimolecular fluorescence complementation (BiFC) assays

Leaves of *N. benthamiana* were infiltrated with *Agrobacterium tumefaciens* GV3101 strains harboring the gene of interest fused to nYFP (N-terminus of YFP) in combination with another gene fused to cYFP (C-terminus of YFP), or an empty vector. The bacteria were kept in infiltration buffer for 2–3 h and mixed with p19 before infiltration. Images were taken on a Zeiss (Germany) LSM 880 confocal microscope 2 d after infiltration.

Extracellular and cytosolic Ca^{2+} measurements

Visualization of extracellular Ca^{2+} distribution using low-affinity cell-impermeable Ca^{2+} fluorescent dye Oregon Green 488 BAPTA-5N Hexapotassium Salt (OGB-5N; cat. no. 06812; Invitrogen) was performed as described previously (Wang *et al.*, 2017). Briefly, wild-type and *cncg20-4* mutant plants were grown hydroponically for 2–3 wk on liquid medium containing 0.1 mM Ca^{2+}. Mature leaves were then detached and their petioles were placed in a solution containing 10 mM Ca^{2+} and OGB-5N. After 4 h staining, the complete leaf blade was visualized under a confocal laser scanning microscope (Zeiss LSM 880). To visualize cytosolic Ca^{2+}, a plasmid for the GCaMP3 reporter controlled by a 35S promoter was transfected into protoplasts isolated from leaves of 4-wk-old plants (Toyota *et al.*, 2018). After overnight incubation, GCaMP3 fluorescence was visualized with GFP excitation at 470 nm and emission at 500–550 nm using a Zeiss 880 confocal laser scanning microscope. Mean fluorescence of the images was calculated using ImageJ software (https://imagej.nih.gov/ij/).

Results

Analysis of Arabidopsis *sped1* as a suppressor of *eds1*

In Arabidopsis accession Columbia (Col), *Pseudomonas syringae* pv *tomato* strain DC3000 delivering the effector AvrRps4 (*Pst AvrRps4*) is recognized by the TNL receptor pair RRS1 (RESISTANCE TO *RALSTONIA SOLANACEARUM*1) and RPS4 (RESISTANCE TO *P. SYRINGAE*4) (Heidrich *et al.*, 2011; Saucet *et al.*, 2015; Ma *et al.*, 2018). Accordingly, Col *eds1-2* null mutant plants display high disease susceptibility to *Pst AvrRps4* due to a loss of RRS1-RPS4 ETI and basal immunity (Bartsch *et al.*, 2006; Cui *et al.*, 2017, 2018). To identify further immunity components, we screened for suppressors of *eds1-2* susceptibility to *Pst AvrRps4* in an EMS-mutagenized population (Cui *et al.*, 2018). From *c.* 650 000 M2 plants, we isolated 21 mutants, named *suppressors of eds1* (*sped*) mutants, with enhanced *Pst AvrRps4* resistance compared to *eds1-2*. Twelve previously described *sped* mutants have independent mutations in *CORONATINE INSENSITIVE 1* (*COI1*) (Cui *et al.*, 2018). *COI1* encodes an F-box protein co-receptor with JAZ (jasmonate-zim-domain) repressors that binds bioactive jasmonoyl-isoleucine (JA-Ile) to initiate jasmonic acid signaling (Sheard *et al.*, 2010). Enhanced bacterial resistance in *eds1 coi1* mutants reflects TNL/EDS1 blocking of bacterial coronatine-antagonized early defense gene expression (Cui *et al.*, 2018; Bhandari *et al.*, 2019). Here, we describe characterization of *sped1*, which is not allelic with *coi1*. Enhanced resistance of *eds1-2 sped1* to *Pst AvrRps4* was confirmed in nonsegregating M3 progeny (Fig. 1a). At 6 d after *Pst AvrRps4* spray inoculation, *eds1-2* seedlings exhibited chlorosis, whereas *eds1-2 sped1* seedlings remained green, resembling wild-type (WT) Col (Fig. 1a). Four- to five-week-old *eds1-2 sped1* plants grown in soil under short-day conditions developed normally (Fig. 1b).

After infiltrating bacteria directly into leaves to bypass stomatal defenses (Xin & He, 2013), *eds1-2 sped1* plants displayed resistance to *Pst AvrRps4* growth that was intermediate between *eds1-2* and WT (Fig. 1c), indicating that the *sped1* mutant partially restores resistance to *Pst AvrRps4* in *eds1-2*. Susceptibility of *eds1-2* to virulent *Pst* DC3000 bacteria was similarly reduced in *eds1-2 sped1* (Fig. 1d), indicating a partial recovery of basal immunity. Expression of the defense marker genes *PR1* and *PR2* in *eds1-2 sped1* plants at 24 h post *Pst AvrRps4* infiltration was similar to WT (Fig. 1e,f). These data show that *sped1* leads to a partial suppression of bacterial disease susceptibility in *eds1-2*.

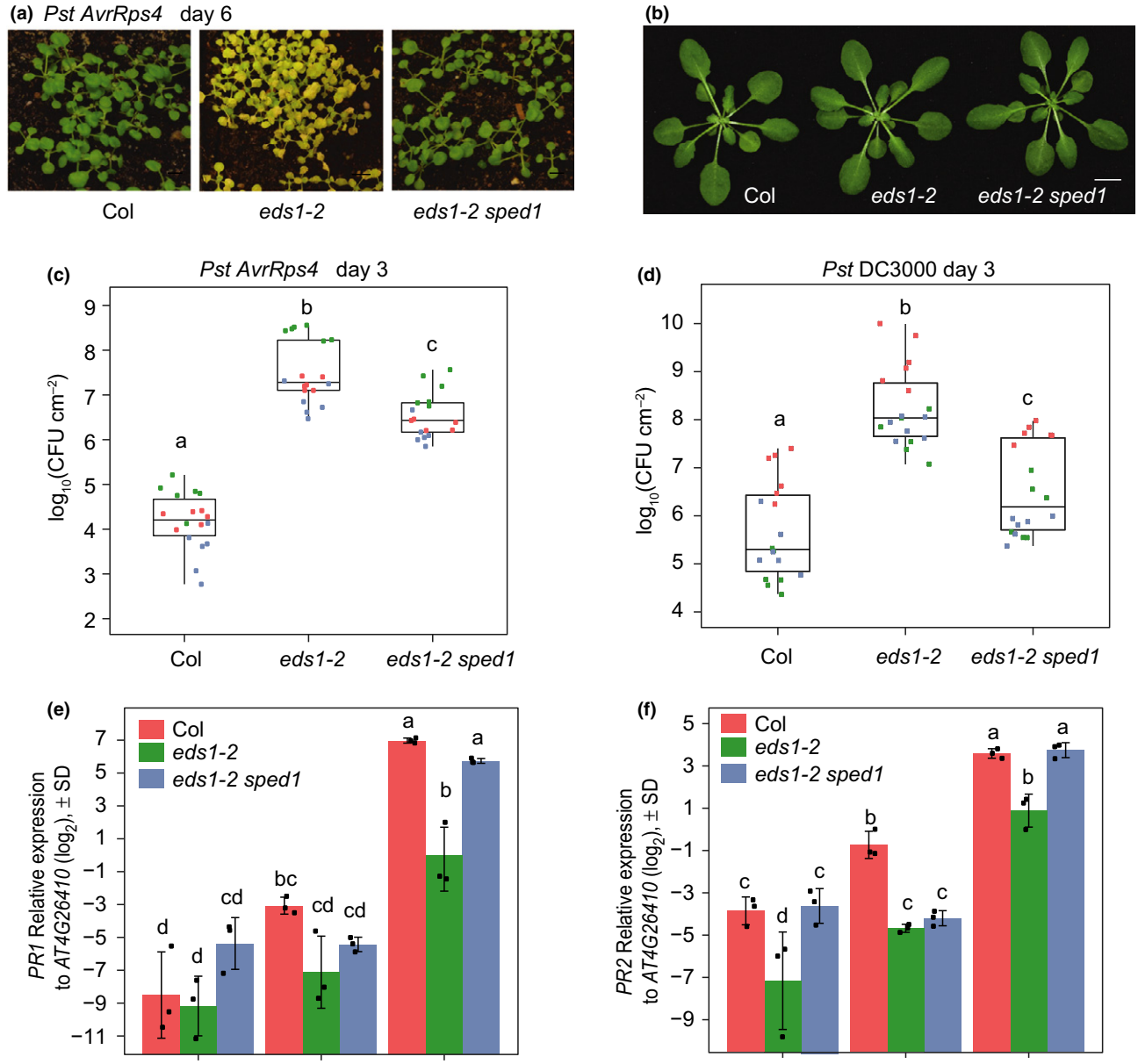

Fig. 1 The *sped1* mutant partially suppresses *eds1-2* susceptibility. (a) Disease symptoms on Arabidopsis Col, *eds1-2* and *eds1 sped1* after spray-inoculation of *Pseudomonas syringe* pv *tomato* DC3000 *AvrRps4* (*Pst AvrRps4*). Two-week-old seedlings grown in soil were spray-inoculated with a bacterial suspension ($OD_{600} = 0.2$). Pictures were taken at 6 d post inoculation (dpi). Bars, 0.5 cm. (b) Rosette morphology of 4-wk-old Col, *eds1-2* and *eds1 sped1* plants grown in soil. Bar, 1 cm. (c, d) Growth of *Pst AvrRps4* (c) or *Pst* DC3000 (d) in leaves of Col, *eds1-2* and *eds1-2 sped1*. Leaves of 4-wk-old plants were infiltrated with bacterial suspensions ($OD_{600} = 0.0002$) and bacterial titers were determined at 3 dpi. Dots with different colors in boxplots represent three independent experiments with six biological replicates in each experiment. The box whiskers indicate variability outside the upper and lower quartiles. Different letters indicate statistical significance ($P < 0.01$) determined by one-way ANOVA followed by Tukey's HSD. CFU, colony-forming units. (e, f) Real-time quantitative polymerase chain reaction (qRT-PCR) analysis of *PR1* (e) and *PR2* (f) expression in Col, *eds1-2* and *eds1-2 sped1* plants at 0 or 24 h post infiltration (hpi) with *Pst AvrRps4*. Four-week-old plants were infiltrated with a bacterial suspension ($OD_{600} = 0.002$). Gene expression was normalized to *AT4G26410*. Values are means ± SD ($n = 3$ biological replicates, indicated by dots in black). Different letters indicate statistical significance ($P < 0.01$) determined by one-way ANOVA followed by Tukey's HSD. The experiments were repeated twice with similar results.

After backcrossing *eds1-2 sped1* with *eds1-2*, F1 progeny displayed similar susceptibility as *eds1-2*. Of 48 F2-generation plants, 34 exhibited *eds1-2*-like and 14 *eds1-2 sped1*-like resistance to *Pst AvrRps4*, consistent with the *sped1* phenotype being caused by a single recessive mutation (expected 3 : 1 ratio of F2 phenotypes, $\chi^2 = 0.444$; $P > 0.5$).

A mutation in *CNGC20* causes *sped1* enhanced immunity

To identify the mutation in *sped1* that partially suppresses *eds1-2* disease susceptibility, we performed whole-genome sequenced-based mapping of 50 F2 progeny from a backcross of *eds1-2 sped1* with *eds1-2*. Two mutations were detected on

chromosome 3 that co-segregated with the *sped1* phenotype. One is in the 3′UTR of *AT3G18350*, annotated as a protein with unknown function. The other is a G-A missense mutation in the fourth exon of *AT3G17700* encoding CYCLIC NUCLEOTIDE-GATED CHANNEL20 (CNGC20) (Kugler *et al.*, 2009; Yu *et al.*, 2019). The G-A mutation results in exchange of leucine^{371} to phenylalanine (L371F) in one of six predicted CNGC20 membrane-spanning domains (Fig. 2a). We denote *sped1* as *cngc20-4*, following three published alleles (Yu *et al.*, 2019).

Of 20 CNGCs in Arabidopsis, CNGC20 and its closest homolog CNGC19 group together with CNGC2 and CNGC4 in one subfamily (Fig. S1a) (Mäser *et al.*, 2001). Sequence alignments show that all CNGC members have leucine at CNGC20^{L371} except CNGC4 and CNGC11, which have a methionine and phenylalanine, respectively, at this position (Fig. 2b). Leucine, methionine and phenylalanine are nonpolar hydrophobic amino acids, suggesting this site is well conserved among Arabidopsis CNGC members. To test whether the L317F mutation in *cngc20-4* causes the *sped1* resistance phenotype, we transformed a C-terminally YFP-tagged wild-type *CNGC20* cDNA transgene driven by a CaMV 35S promoter (*CNGC20-YFP*) into *eds1-2 cngc20-4*. We noted that the *eds1-2 cngc20-4* mutant has delayed flowering and a shorter primary inflorescence shoot compared to WT or *eds1-2* (Fig. S1b). Of 21 *CNGC20-YFP eds1-2 cngc20-4* T1 transgenic lines examined, 18 displayed flowering times and primary inflorescence shoot lengths resembling WT (Fig. S1b). Six randomly selected independent homozygous lines carrying the *CNGC20-YFP* transgene had *eds1-2*-like susceptibility to *Pst AvrRps4* (Figs 2c, S1c), indicating that *CNGC20-YFP* complements *sped1* in an *eds1-2* background. We concluded that *CNGC20^{L371F}* underlies the observed *sped1* phenotypes.

CNGC20^{L371F} produces autoimmunity and enhances NLR-triggered cell death

A *cngc20-4* (*CNGC20^{L371F}*) single mutant was obtained after backcrossing *eds1-2 cngc20-4* with Col. *Cngc20-4* plants were stunted, with slightly narrow, curling leaves compared to WT (Fig. 2d). The *cngc20-4* developmental phenotype was different to that of *dnd1*, a null mutant of *CNGC2* (Fig. 2d) (Clough *et al.*, 2000). *Cngc20-4* plants constitutively expressed *PR1* and *PR2* (Fig. 2e) and had increased resistance to virulent *Pst* DC3000 (Fig. 2f), indicating that *cngc20-4* causes autoimmunity.

We did not observe lesions in 5-wk-old *cngc20-4* plants grown in soil, indicating that *cngc20-4* does not lead to spontaneous cell death under our growth conditions (Fig. S1d). We then examined HR-related leaf cell death in *cngc20-4* in TNL (RRS1/RPS4) and CNL (RPS2) ETI responses by quantifying ion leakage over 24 h after *Pst AvrRps4* or *Pst AvrRpt2* infiltration. In these assays, both TNL- and CNL-triggered cell death was accelerated and enhanced in *cngc20-4* compared to WT (Figs 2g, S1e). By contrast, a *CNGC20* T-DNA insertion line, *cngc20-1* (Salk_129133) (Kugler *et al.*, 2009), was indistinguishable from WT in morphology (Fig. 2d), resistance to *Pst* DC3000 (Fig. 2f) and NLR-triggered cell death in response to *Pst AvrRps4* or *Pst AvrRpt2* (Figs 2g, S1e). Similarly, a *cngc19-1* (Salk_027306) mutant resembled WT plants (Fig. S1f) and displayed WT basal resistance to *Pst* DC3000 (Fig. S1g).

Transient expression of CNGC19, CNGC20, CNGC20^{L371F} or a combination of these in *N. benthamiana* did not produce visible lesions on leaves. However, co-expression of CNGC19 with CNGC20 or CNGC20^{L371F} enhanced bacterial effector protein XopQ-induced ion leakage (Fig. S2a). XopQ is an effector of *Xanthomonas campestris* pv *vesicatoria* (*Xcv*) which triggers TNL Roq1- and *EDS1*-dependent ETI cell death in *N. benthamiana* (Adlung *et al.*, 2016). Transiently expressed CNGC20^{L371F}, but not CNGC20 or CNGC19, partially rescued *Nbeds1a* susceptibility to *Xcv* (Fig. S2b). Together, these results show that the L371F exchange in *cngc20-4* creates a CNGC20 gain-of-function (mis-regulated) variant which leads to autoimmunity in Arabidopsis.

Cngc20-4 mutant plants exhibit enhanced PTI responses

Because the *cngc20-4* mutant showed increased basal resistance to virulent *Pst* DC3000, we investigated whether *cngc20-4* PTI responses are enhanced. Application of Pep1, a 23-aa endogenous peptide that functions as a DAMP in Arabidopsis (Liu *et al.*, 2013), led to increased root growth inhibition in *cngc20-4* and *eds1-2 cngc20-4*, but not *cngc20-1* or *cngc19-1* seedlings, compared to WT (Figs 3a, S3a). Similarly, flg22, a 22-aa PAMP peptide from bacterial flagellin, induced stronger root growth inhibition in *cngc20-4* and *eds1-2 cngc20-4* seedlings compared to WT (Figs S3a; S3b). Both flg22 and Pep1 elicited a higher ROS burst in *cngc20-4* and *eds1-2 cngc20-4* seedlings compared to WT (Figs 3b, S3c). The Pep1-elicited, but not flg22-elicited, *cngc20-4* enhanced ROS burst was further increased in *eds1-2 cngc20-4* (Fig. 3b). This suggests that *cngc20-4* deregulated immunity dampens the Pep1 DAMP response in an *EDS1*-dependent manner, via an unknown mechanism. Notably, flg22-induced activation of MAPKs in *cngc20-4* was similar to WT (Fig. S3d). These data show that *cngc20-4* enhances certain PAMP and DAMP outputs.

Cngc20-4 autoimmunity utilizes *EDS1* and SA pathways redundantly

Because *EDS1* and *ISOCHORISMATE SYNTHASE1* (*ICS1*)-generated SA pathways work in parallel in Arabidopsis ETI and basal immunity (Venugopal *et al.*, 2009; Cui *et al.*, 2017), we assessed the effect of mutating *EDS1* and *ICS1* together on *cngc20-4* enhanced immune responses. For this, we selected a *sid2-1 cngc20-4* double and an *eds1-2 sid2-1 cngc20-4* triple mutant by crossing *eds1-2 cngc20-4* with *sid2-1* (mutated in *ICS1*). The *cngc20-4* developmental defects were partially suppressed by *eds1-2* or *sid2-1* and were almost fully suppressed in the *eds1-2 sid2-1 cngc20-4* triple mutant (Figs 4a, S4a). Total SA quantitation in leaves showed that *cngc20-4* plants constitutively accumulated more SA, while *eds1-2 cngc20-4* and *sid2-1 cngc20-4* accumulated similar quantities of SA as WT

(Fig. S4b). Although the flg22-induced ROS burst was reduced in *sid2* compared with WT (Fig. S4c) (Yi *et al.*, 2014), it was nevertheless increased by the presence of *cngc20-4* in *sid2-1* (Fig. S4c). In *Pst* DC3000 growth assays, *eds1-2*, *sid2-1* and *eds1-2 sid2-1* were all highly susceptible, whereas *cngc20-4* was more resistant than WT (Fig. 4b). The *cngc20-4* mutation increased resistance to *Pst* DC3000 in *eds1-2* and *sid2-1* single mutant backgrounds, but not in the *eds1-2 sid2-1* double mutant (Fig. 4b). These data show that *EDS1* and *ICS1* contribute redundantly to *cngc20-4* autoimmunity. Combining

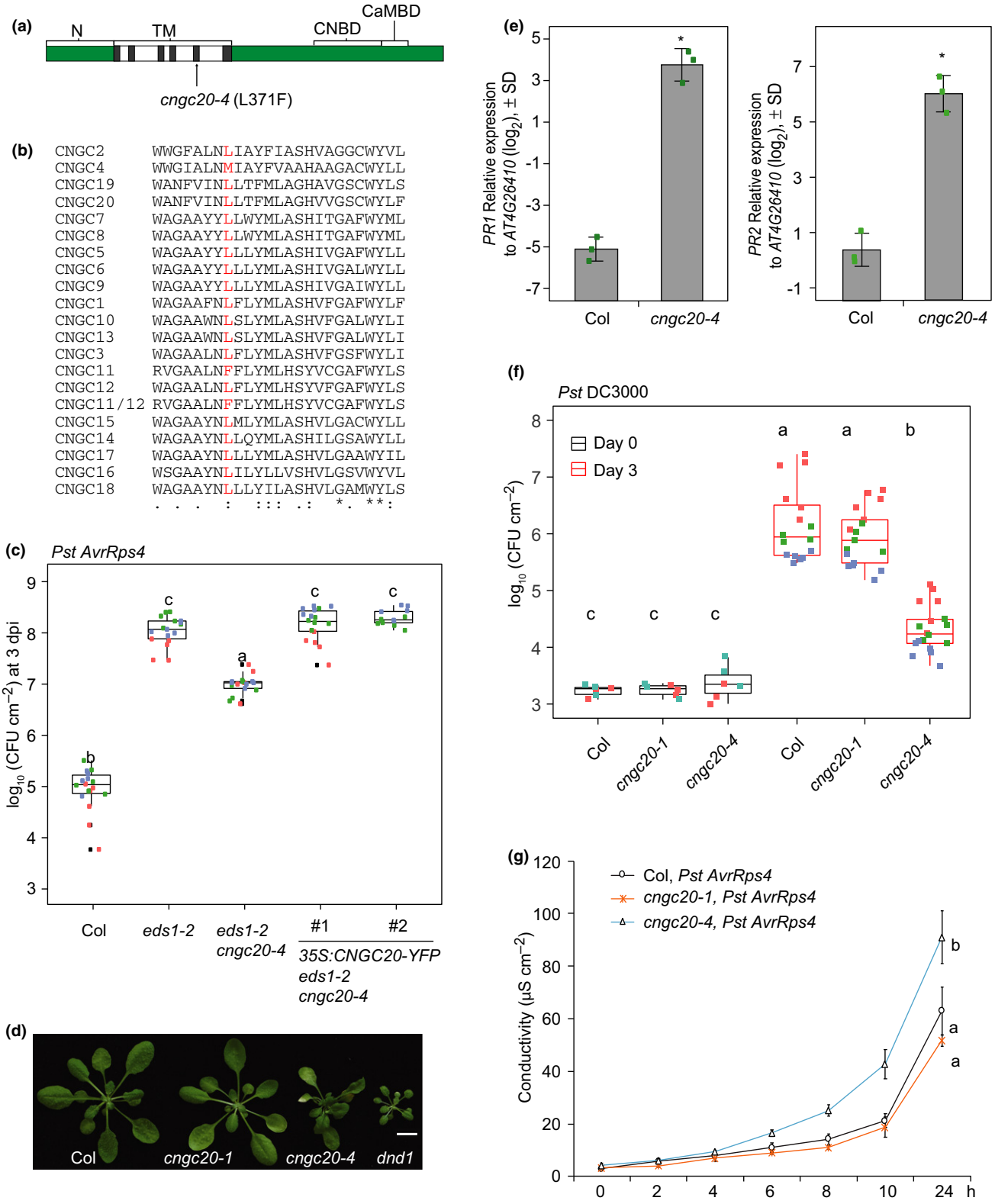

eds1-2 and *sid2-1* mutations also suppressed *cngc20-4* enhanced flg22-induced root growth inhibition to the same level as WT (Fig. 4c). By contrast, *cngc20-4* enhanced root growth inhibition in response to Pep1 was not suppressed by *eds1-2 sid2-1* (Fig. S4d). Together, these data show that *cngc20-4* engages both *EDS1* and SA for autoimmunity.

The *cngc20-4* mutation mis-regulates calcium channel ion flux

A recent study showed that CNGC20 is a calcium channel that regulates cell death in a *bak1/serk4* mutant (Yu *et al.*, 2019). The ion channels formed by CNGCs are tetramer protein complexes (Chin *et al.*, 2013; Pan *et al.*, 2019). Based on the protein crystal structure of human potassium/sodium hyperpolarization-activated cyclic nucleotide-gated channel1 (HCN1) (Lee & MacKinnon, 2017), a structural model for CNGC20 (https://swissmodel.expasy.org) shows that four protein molecules oligomerize to form a potential pore via transmembrane domains S5 and S6 (Fig. S5). CNCG20 residue L371 is positioned on transmembrane domain S5 facing into the pore (Fig. S5), suggesting that the *cngc20-4* L371F mutation might affect channel activity. To test this, we used a membrane-impermeable low-affinity Ca^{2+} fluorescent dye, Oregon Green BAPTA 488 5N (OGB-5N), to visualize plant extracellular Ca^{2+} accumulation *in vivo* (Wang *et al.*, 2017). The method was developed to detect Ca^{2+} over-accumulation in the extracellular spaces of *dnd1* leaves (Wang *et al.*, 2017). In plants, Ca^{2+} is absorbed through the root, uploaded into the xylem, and further transported to the leaves, where it is unloaded from the xylem and re-distributed into leaf cells (White, 2001; Gilliham *et al.*, 2011). Wild-type and *cncg20-4* mutant plants were grown hydroponically for 2–3 wks on liquid medium containing 0.1 mM Ca^{2+}. Mature leaves were then detached and their petioles were placed into a solution containing 10 mM Ca^{2+} and OGB-5N. After 4 h staining, we detected extracellular Ca^{2+}-dependent green fluorescence in the vasculature of Col and *eds1-2* leaves (Fig. 5a,b). Under the same conditions, we observed a high green fluorescence signal in *dnd1* leaves (Fig. 5a, b), consistent with a previous report (Wang *et al.*, 2017). By contrast, only weak fluorescent signals were observed in *cngc20-4* and *eds1-2 cngc20-4* veins (Fig. 5a,b). We reasoned that reduced extracellular Ca^{2+} accumulation in *cngc20-4* lines might be caused by increased Ca^{2+} influx via $CNCG20^{L371F}$ into the cytoplasm. Next we used a GFP-based fluorescent Ca^{2+} indicator, GCaMP3, to monitor cytosolic Ca^{2+} in a protoplast transient expression assay (Toyota *et al.*, 2018). A higher GFP fluorescent signal was observed in *cngc20-4* and *eds1-2 cngc20-4* compared to WT, *eds1-2* and *dnd1* protoplasts (Fig. 5c,d). Taken together, these results suggest that increased Ca^{2+} channel activity in *cngc20-4* leads to higher cytosolic Ca^{2+} accumulation, potentially explaining the *cngc20-4* autoimmunity phenotype. Thus, *cngc20-4* appears to have a mis-regulated Ca^{2+}-permeable ion channel.

$CNGC20^{L371F}$ does not disrupt homomeric complexes or heteromeric association with CNGC19

The CNGC20 structural model suggests it forms a membrane-spanning tetramer complex producing a channel or pore (Fig. S5). Because the *cgnc20-4* mutant displays increased cytosolic Ca^{2+} accumulation and autoimmunity, we tested the subcellular localization and interactions of CNGC20 and $CNGC20^{L371F}$ proteins. Transiently expressed CNGC20-YFP and $CNGC20^{L371F}$ localized to the plasma membrane in Arabidopsis protoplast transfection assays (Fig. 6a). CNGC20 and CNGC19 were recently shown to form homodimer and heterodimer channel complexes that transport Ca^{2+} (Yu *et al.*, 2019). Therefore, we examined whether CNGC20 self-associates and/or forms a heteromeric complex with CNGC19, and the effects of L371F mutation on these interactions. In BiFC experiments, both CNGC20 and $CNGC20^{L371F}$ were able to self-associate and interact with CNGC19 (Fig. 6b). In co-immunoprecipitation (Co-IP) assays of transiently expressed proteins in Arabidopsis protoplasts, CNGC20-HA co-purified with CNGC20-YFP, and CNGC19-HA co-purified with $CNGC20^{L371F}$-YFP or CNGC20-YFP (Fig. 6c,d). These results show that the $CNGC20^{L371F}$ mutation does not disrupt CNGC20 formation of homomeric complexes or heteromeric association with CNGC19.

Fig. 2 Mutation in *CNGC20* is responsible for *sped1* phenotypes. (a) Scheme showing CNGC20 domains and position of L371F mutation. CaMBD, calmodulin binding domain; CNBD, cyclic nucleotide binding domain; N, N-terminus; TM, transmembrane domain (six of which are indicated in gray). (b) Conservation of $CNGC20^{L371}$ in S5 transmembrane domains in the CYCLIC NUCLEOTIDE-GATED CHANNEL (CNGC) family. Sequence alignment of 20 CNGCs in Arabidopsis was performed in MUSCLE (https://www.ebi.ac.uk/Tools/msa/muscle/). Conserved $CNGC20^{L371}$ residue is indicated in red. Asterisks indicate identical amino acids. Colons indicate conserved amino acids. Dots indicate less conserved amino acids. (c) Growth of *Pseudomonas syringe* pv *tomato* DC3000 *AvrRps4* (*Pst AvrRps4*) in leaves of Col, *eds1-2*, *eds1-2 sped1* and two *35S:CNGC20-YFP* complementation lines. Leaves of 4-wk-old plants were infiltrated with bacterial suspensions ($OD_{600} = 0.0002$). Dots with different colors in boxplots represent three independent experiments with six biological replicates in each experiment. The box whiskers indicate variability outside the upper and lower quartiles. Different letters indicate statistical significance ($P < 0.01$) determined by one-way ANOVA followed by Tukey's HSD. CFU, colony-forming units; dpi, days post inoculation. (d) Morphology of 4-wk-old plants of the indicated genotypes grown in soil. Bar, 1 cm. (e) Basal expressions of *PR1* and *PR2* expression in leaves of 4-wk-old Col and *cngc20-4* plants measured by real-time quantitative polymerase chain reaction (qRT-PCR), normalized to *AT4G26410*. Error bars represent means ± SD ($n = 3$ biological replicates, indicated by dots in green); asterisks indicate statistical significance (*, $P < 0.01$) determined by Student's *t*-test. The experiment was repeated twice with similar results. (f) Growth of *Pst* DC3000 in Col, *cngc20-1* and *cngc20-4* leaves. Experiments were performed as described in (c), except three biological replicates were used for day 0 measurements. CFU, colony-forming units. (g) Quantitative ion leakage assays over 24 h in leaf discs of 4-wk-old Col, *cngc20-1* and *cngc20-4*, after infiltration with *Pst AvrRps4* ($OD_{600} = 0.2$). Error bars represent means ± SD ($n = 4$ biological replicates). Different letters indicate statistical significance ($P < 0.01$) at 24 h determined by one-way ANOVA followed by Tukey's HSD. The experiment was repeated three times with consistent results.

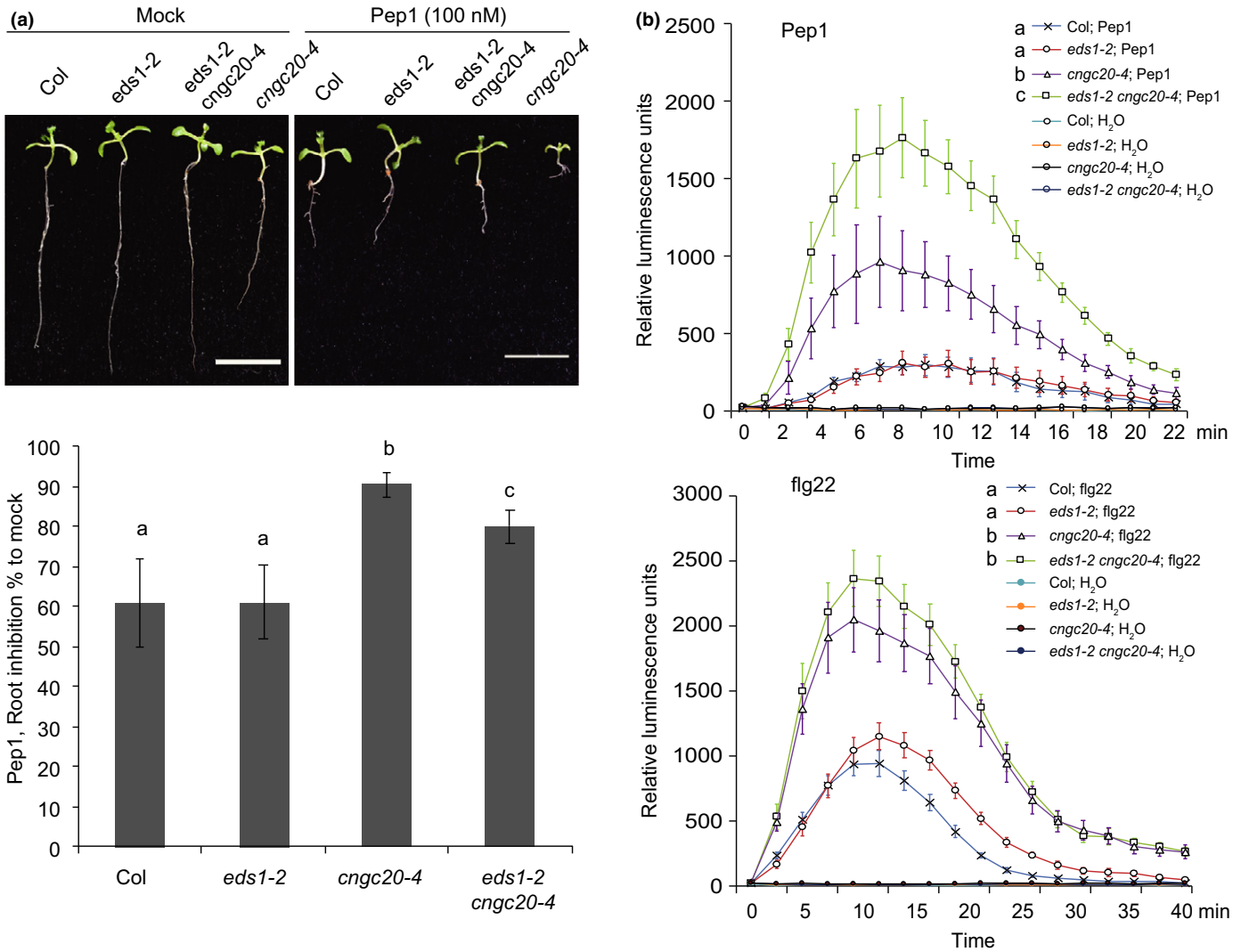

Fig. 3 *cngc20-4* enhances PAMP-induced growth inhibition and reactive oxygen species (ROS) burst. (a) Root growth inhibition of Arabidopsis seedlings exposed to 100nM Pep1 for 7 d. Growth inhibition rates were calculated as the percentage difference between mock and Pep1-treated root length over root length of mock treatment (average ± SD, $n = 30$). Different letters indicate statistical significance ($P < 0.01$) determined by one-way ANOVA followed by Tukey's HSD. Bars, 1 cm. (b) Enhanced Pep1- and flg22-induced H_2O_2 production in plants containing *cngc20-4*. Results shown are representative of three independent experiments. Each data point consists of six to eight replicates. Values are means ± SD. Different letters indicate statistical significance ($P < 0.01$) determined by one-way ANOVA followed by Tukey's HSD. All experiments were repeated three times with consistent results.

BIK1 phosphorylates and stabilizes CNGC20

CNGC2 and CNGC4 Ca^{2+} channel activity is regulated by BIK1 (Tian *et al.*, 2019). We tested whether BIK1 interacts with CNGC20. In BIFC experiments, CNGC20 associated with BIK1 at the plasma membrane (Fig. 7a). In IP assays, BIK1-HA co-precipitated with CNGC20-YFP in the presence and absence of a flg22 stimulus, suggesting a constitutive interaction (Fig. 7b). BIK1-HA also associated with CNGC20^{L371F}-YFP (Fig. 7c), indicating that this mutation does not abolish interaction between BIK1 and CNGC20. We found that the C-terminal cytosolic domain of CNGC20 (CNGC20CT) interacts with BIK1 in IP experiments (Fig. 7d) and in *in vitro* pull-down assays (Fig. 7e), suggesting direct association between BIK1 and CNGC20CT. To test whether BIK1 directly phosphorylates CNGC20CT, we performed an *in vitro* phosphorylation assay using proteins purified from *E. coli*. Phosphorylation of GST-CNGC20CT was detected with anti-phosphor-threonine antibody when incubated with GST-BIK1, but not with GST alone (Fig. 7f), indicating that CNGC20CT can be phosphorylated by BIK1. In an *in vivo* phosphorylation assay, we failed to detect CNGC20 phosphorylation on Phos-tag gels when it was co-expressed with BIK1. After transient expression and purification of CNGC20-FLAG using IP with anti-FLAG agarose from Arabidopsis protoplasts and a 15 min flg22 treatment, CNGC20-FLAG was probed on a Western blot with anti-phosphor-threonine antibody to detect possible CNGC20 phosphorylation. In these assays, co-expression with BIK1, but not with a kinase-dead BIK1^{D202A} mutant (Laluk *et al.*, 2011), enhanced phosphorylation of CNGC20 (Fig. 7g). In a cell-free protein stability assay, CNGC20CT-FLAG protein accumulation decreased gradually in *bik1* but not in WT Col total protein extracts over a 30-min

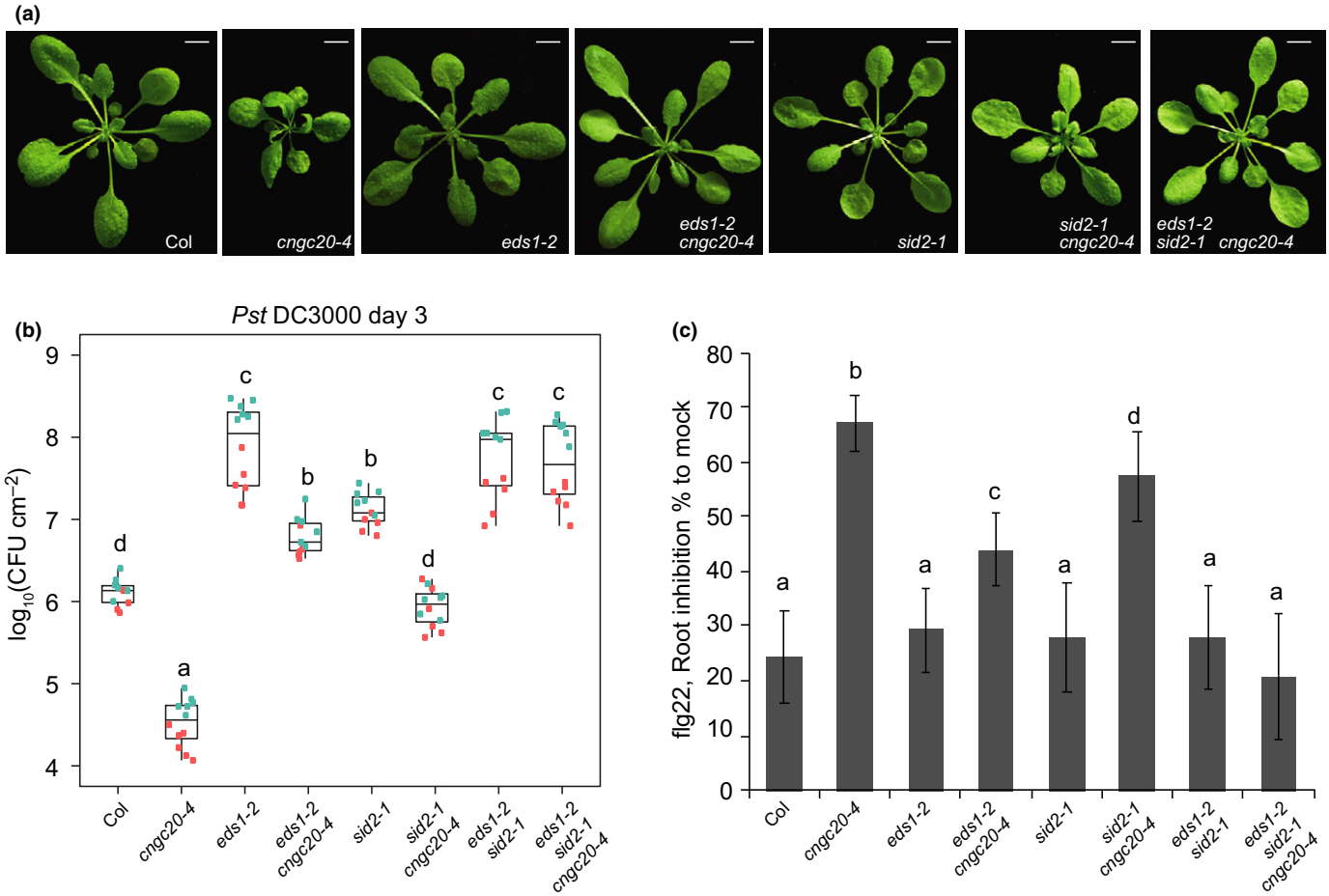

Fig. 4 *cngc20-4*-enhanced immunity is dependent on *EDS1* and salicylic acid (SA). (a) Morphology of 4-wk-old plants of the indicated genotypes. Bars, 1 cm. (b) Growth of *Pseudomonas syringe* pv *tomato* DC3000 in leaves of the indicated genotypes. Leaves of 4-wk-old plants were infiltrated with bacterial suspensions ($OD_{600} = 0.0002$) and bacterial titers were determined at 3 d post inoculation. The same color dots in boxplots represent six biological replicates in one of the two independent experiments. The box whiskers indicate variability outside the upper and lower quartiles. Different letters indicate statistical significance ($P < 0.01$) determined by one-way ANOVA followed by Tukey's HSD. CFU, colony-forming units. (c) Root growth inhibition of Arabidopsis seedling exposed to 200nM flg22 for 7 d. Growth inhibition rates were calculated as the percentage of the root length difference between flg22 and mock treatment over root length of mock treatment (mean ± SD, $n = 30$). Different letters indicate statistical significance ($P < 0.01$) determined by one-way ANOVA followed by Tukey's HSD. The experiment was repeated twice with consistent results.

time course (Fig. 7h), indicating that BIK1 likely stabilizes CNGC20. As a control, accumulation of YFP-FLAG was not affected in this assay (Fig. 7h). Together, these data provide evidence that BIK1 interacts with, phosphorylates and stabilizes CNGC20 protein.

Discussion

Calcium is an essential secondary messenger in plant PTI and ETI (Grant *et al.*, 2000; Moeder *et al.*, 2019), but mechanisms controlling Ca^{2+} influx into cells during these immune responses have emerged only recently (Tian *et al.*, 2019; Yu *et al.*, 2019; Wang *et al.*, 2019b). In Arabidopsis, two CNGC pairs, CNGC2 and 4 and CNGC20 and 19, were characterized as plasma membrane-localized Ca^{2+}-permeable channels with immunity signaling roles (Tian *et al.*, 2019; Yu *et al.*, 2019). Whereas a CNGC2-4 heteromeric complex is necessary to generate an active Ca^{2+}channel that promotes PTI responses (Tian *et al.*, 2019), CNGC20 exhibits autonomous Ca^{2+} channel activity which can be augmented by CNGC19 to maintain Ca^{2+} homeostasis (Yu *et al.*, 2019). Hence, different CNGCs and CNGC combinations appear to make distinctive contributions to the regulation of immunity. In this study, we report the isolation and characterization of an Arabidopsis recessive mutant, *cngc20-4*, which displays autoimmunity dependent on the combined actions of *EDS1*, an early component of ETI, and SA, a hormone potentiator of PTI and ETI responses (Figs 2, 4) (Zhang & Li, 2019). Accordingly, *cngc20-4* plants displayed elevated ROS responses to the PAMP flg22 and DAMP Pep1 (Fig. 3b), and accelerated host cell death in TNL and CNL-triggered ETI (Figs 2g, S1e). We find that an L371F exchange in *cngc20-4* on a predicted transmembrane surface facing into the CNGC20 channel pore causes Ca^{2+} channel mis-regulation and increased cytosolic Ca^{2+} accumulation (Fig. 5). We further establish that BIK1 interacts, phosphorylates and stabilizes CNGC20 (Fig. 7). Together, our data show that a mis-regulated CNGC20 Ca^{2+} channel increases both PTI and

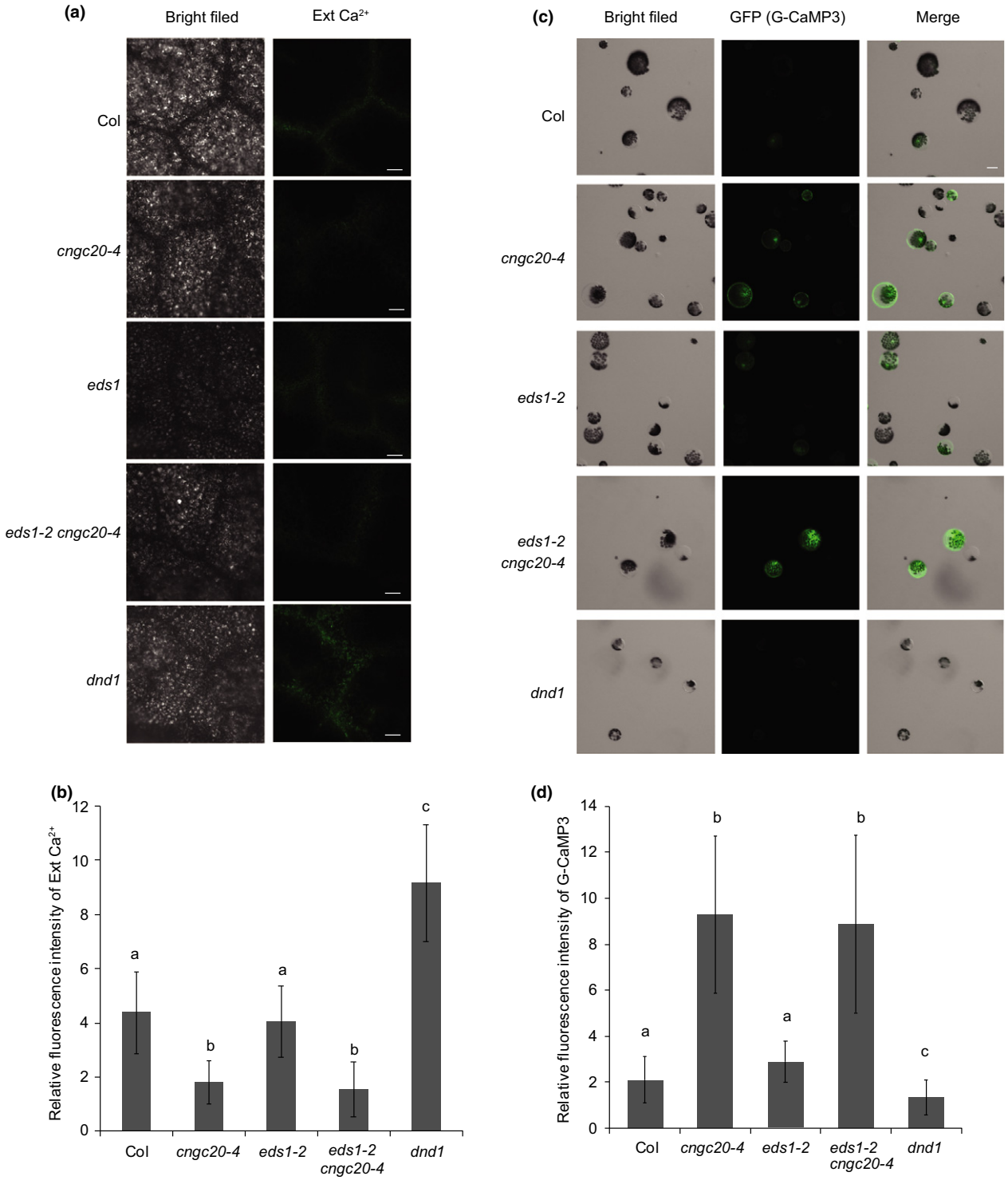

Fig. 5 Confocal microscopy of extracellular and cytosolic Ca^{2+} in Arabidopsis. (a) Fluorescence microscopy of extracellular Ca^{2+} in leaves of Col, *cngc20-4*, *eds1-2*, *eds1-2 cngc20-4* and *dnd1*. Plants were grown hydroponically in 0.1 mM Ca^{2+} for 3 wk. Fully expanded leaves were detached and inserted into 200 µl tubes with growth medium in the presence of 10 mM Ca^{2+} and 20 µM Ca^{2+}-dependent fluorescent dye OGB-5N. Images were taken at 4 h after OGB-5N treatment. Bars, 100 µm. (b) Quantitative analysis of OGB-5N fluorescence intensity of (a) using ImageJ software. Error bars represent ± SD ($n = 15$ areas). Different letters indicate statistical significance ($P < 0.01$) determined by one-way ANOVA followed by Tukey's HSD. (c) Fluorescence microscopy of cytosolic green fluorescent protein (GFP) of the Ca^{2+} reporter GCaMP3 in protoplasts from the indicated genotypes. An equal amount of GCaMP3 plasmid was transfected into protoplasts of each line. Basal GFP fluorescence was captured by confocal microscopy 16 h after transformation. Bars, 10 µm. (d) Quantitative analysis of GFP fluorescence intensity of (c) using ImageJ software. Error bars represent ± SD ($n = 20$ protoplasts). Different letters indicate statistical significance ($P < 0.01$) determined by one-way ANOVA followed by Tukey's HSD. All experiments were repeated three times with consistent results.

ETI outputs via *EDS1* and SA signaling pathways (Fig. S6). Hence, tightly controlled CNGC20 Ca^{2+} channel activity is crucial for immunity homeostasis and pathogen resistance.

Typically, CNGCs contain a cytosolic N-terminus, six transmembrane helices (S1–S6) with a pore-forming region spanning S5 to S6, and a C-terminal cytosolic tail with a cyclic nucleotide binding domain and a calmodulin-binding domain (Leng *et al.*, 2002; Zelman *et al.*, 2012) (Fig. 2a). The L371F mutation in *cngc20-4* is located in the S5 transmembrane domain, and this residue is conserved among CNGCs in Arabidopsis (Figs 2a,b, S5). An L371F exchange might lead to enhanced ion channel activity formed by S5 and S6 domains in the tetrameric CNGC20 protein complexes (Fig. S5). Indeed, Ca^{2+} accumulation in *cngc20-4* was lower in vascular tissues but higher in the cytosol of cells (Fig. 5), supporting the notion that $CNGC20^{L371F}$ forms a mis-regulated Ca^{2+} channel, leading to higher Ca^{2+} influx from the cell exterior to the cytoplasm.

A similar autoimmunity phenotype to *cngc20-4* was observed in Arabidopsis *cpr22*, a rare gain-of-function mutant caused by a 3-kb deletion that fuses *CNGC11* with adjacent *CNGC12* to generate a *CNGC11/12* chimera (Yoshioka *et al.*, 2006). Notably, the F371 residue we identify in *cngc20-4* corresponds to F205 in *CNGC11/12* (Fig. 2b) (Yoshioka *et al.*, 2006). Elevated cytosolic Ca^{2+} was also observed in *cpr22* plants using a Ca^{2+}-sensitive

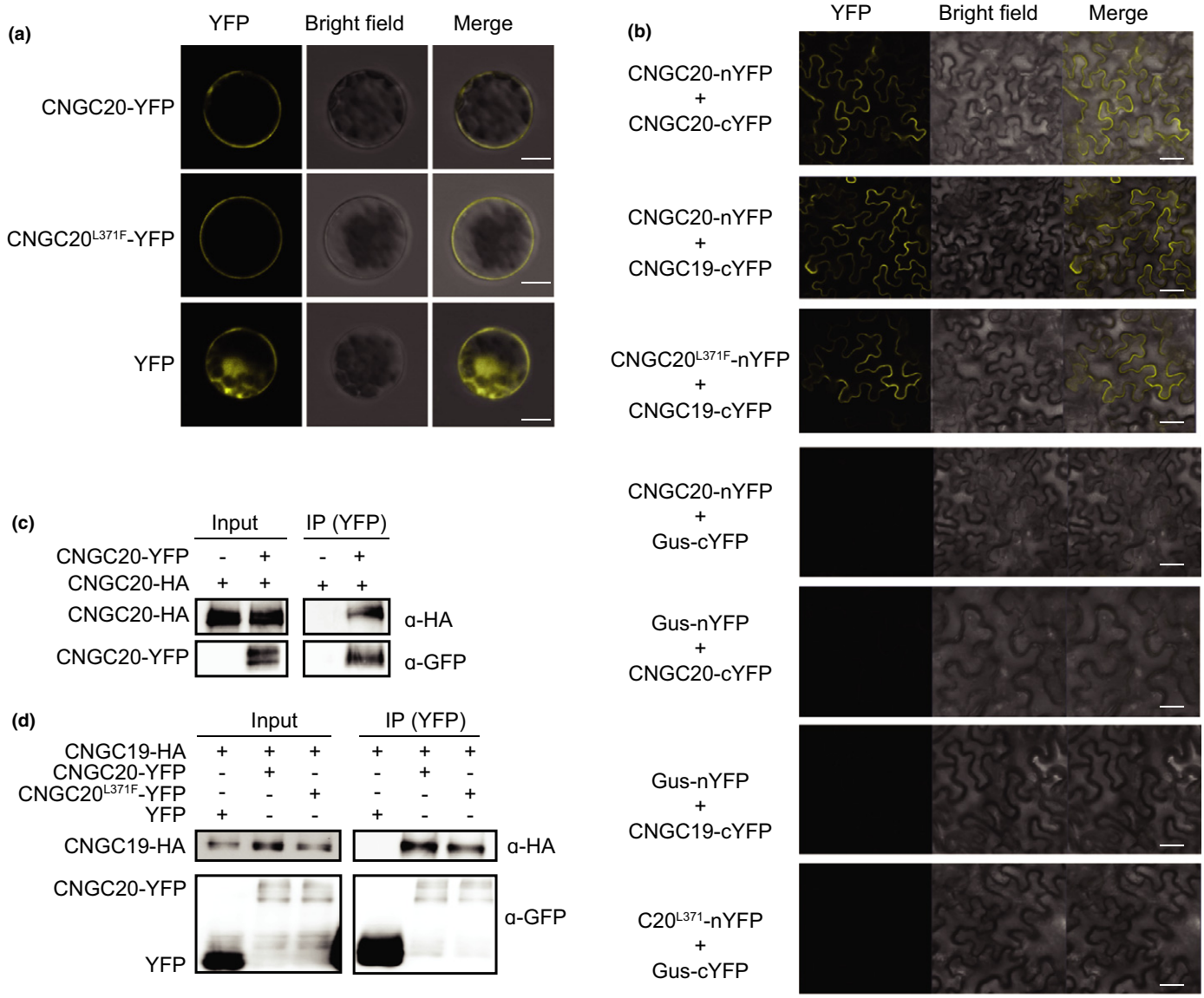

Fig. 6 CNGC20 and CNGC19 form homo- and heteromeric protein complexes. (a) CNGC20-YFP and $CNGC20^{L371F}$-YFP locate to the plasma membrane in Arabidopsis Col protoplasts. YFP-tagged proteins were transiently expressed in protoplasts by polyethylene glycol (PEG)-mediated transformation with plasmid DNA. Images were captured using a confocal microscope 16 h after transformation. Bars, 10 µm. (b) Interactions between CNGC20, $CNGC20^{L371F}$ and CNGC19 in *Nicotiana benthamiana*, revealed by split yellow fluorescent protein (YFP) assays. *N. benthamiana* leaves were co-infiltrated with *Agrobacteria* containing the indicated genes with C-terminal cYFP or nYFP tags on T-DNA. Images were captured using a confocal microscope 2 d after transformation. Bars, 100 µm. (c, d) Co-immunoprecipitation (Co-IP) analysis of interactions between CNGC20, $CNGC20^{L371F}$ and CNGC19 at 16 h after transfection of *Arabidopsis* Col protoplasts. Proteins in total extracts (labelled 'Input') and after IP with GFP-trap beads ('IP (YFP)') were detected on immunoblots using α-HA or α-GFP antibodies. All experiments were repeated three times with consistent results.

fluorescent reporter GCaMP3 (Moeder *et al.*, 2019). In contrast to *cngc20-4*, *cpr22* is a dominant mutation causing spontaneous lesions. Although *cpr22*-induced resistance to bacterial infection required *EDS1*, *cpr22*-associated spontaneous cell death, stunting, leaf curling, elevated SA accumulation and constitutive *PR1* expression were independent of *EDS1* (Yoshioka *et al.*, 2006). Transiently expressed CNGC19 with CNGC20 or CNGC20^{L371F} in *N. benthamiana* enhanced XopQ-induced ion leakage (Fig. S2a), suggesting that CNGC19 and CNGC20 protein complexes form a functional ion channel which can promote

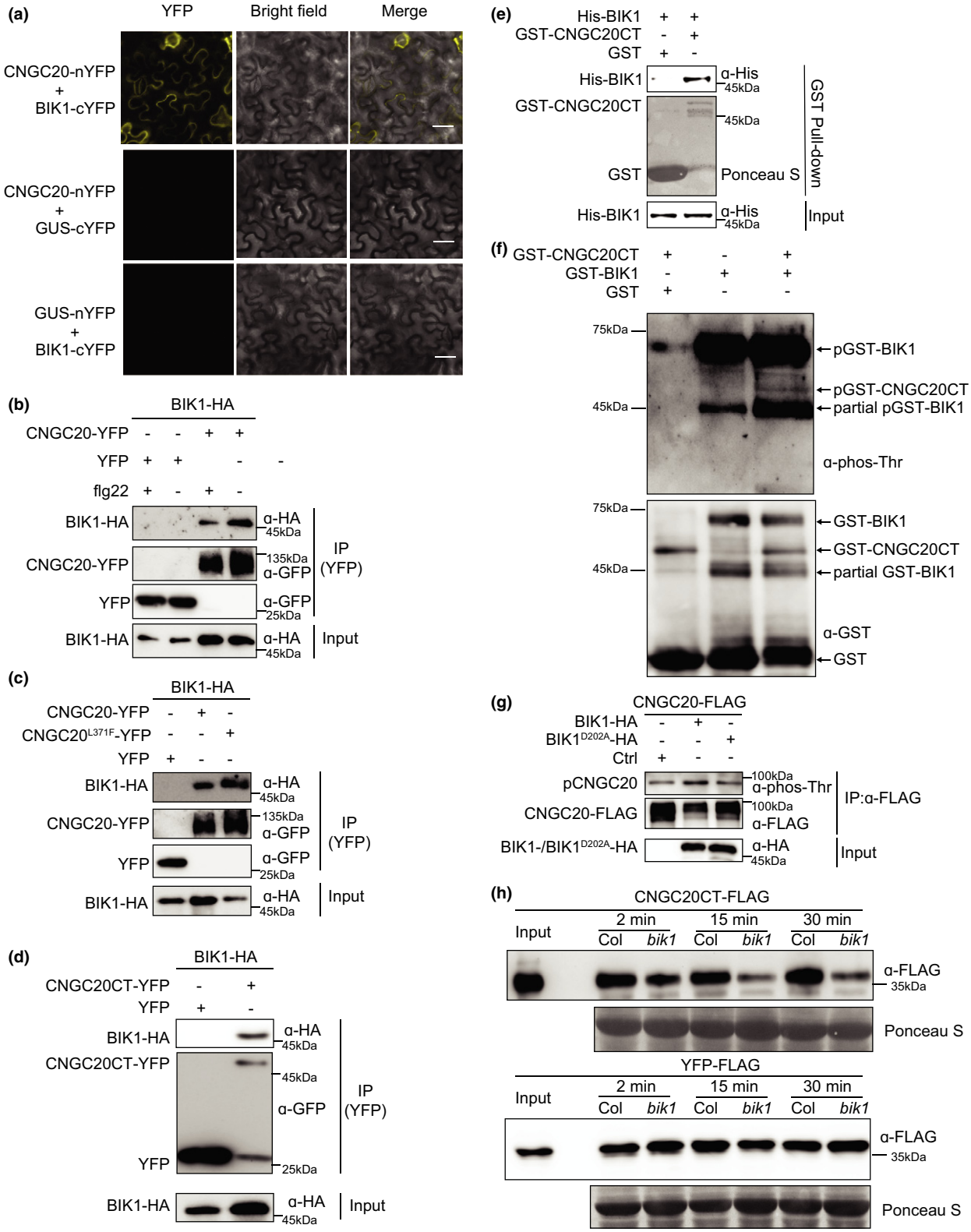

ETI-related host cell death. Thus, although we do not understand the biochemistry underlying recessive *cngc20-4* inheritance in Arabidopsis, it is likely that the L371F exchange creates a weakly mis-regulated protein which is partially constrained within a complex by WT CNGC19 or CNGC20 in a heterozygote. Put together, these data suggest that the conserved L371 of CNGC20 is an important site for regulation of CNGC ion channel activity.

Arabidopsis BAK1 and SERK4 function as coreceptors of cell surface-resident receptor-like kinase PRRs controlling plant growth, development and immune responses (Liang & Zhou, 2018). *BAK1* and *SERK4* also redundantly and negatively regulate plant cell death (He *et al.*, 2007; Kemmerling *et al.*, 2007). Yu *et al* (2019) reported that BAK1 interacts with and phosphorylates CNGC20 to promote CNGC20 degradation and maintain Ca^{2+} and cell death homeostasis (Yu *et al.*, 2019). Accordingly, CNGC20 and CNGC19 over-accumulation in a *bak1/serk4* mutant was associated with increased Ca^{2+} influx and cell death (Yu *et al.*, 2019). Pep2 (DAMP)-induced root growth inhibition was strongly enhanced in an Arabidopsis *bak1* mutant compared to WT, and loss-of-function mutations in *PEPR1* and *PEPR2* (the Pep1-binding receptors) suppressed *bak1* cell death (Yamada *et al.*, 2016). The *pepr* mutations also compromised HR cell death mediated by Arabidopsis CNL receptor RPS2 (Ma *et al.*, 2012), indicating involvement of PEPR signaling in ETI. Emerging data point to mutual potentiation between PTI and ETI receptor systems in conferring robust bacterial resistance (Ngou *et al.*, 2020; Yuan *et al.*, 2020). Our results are consistent with a dichotomy between flg22 (PAMP) and Pep1 (DAMP) signaling because increased cytosolic Ca^{2+} in *cngc20-4* correlated with an enhanced DAMP (Pep1)-triggered ROS burst, root growth inhibition (Fig. 3) and enhanced RPS4- and RPS2-triggered ETI cell death (Figs 2g, S3e). Our findings suggest that elevated Ca^{2+} influx, caused by $CNGC20^{L371F}$ in *cngc20-4* or CNGC20/19 over-accumulation in *bak1*, sensitizes PEPR-mediated DAMP signaling, resulting in enhanced NLR-mediated ETI cell death in *cngc20-4* and cell death in *bak1* (Yamada *et al.*, 2016; Yu *et al.*, 2019). It is possible that PEPR1 signaling is more responsive to and amplifiable by elevated cytosolic Ca^{2+} than FLS2 signaling, because the combined loss of *EDS1* and SA (*ICS1*) pathways reduced *cngc20-4* enhanced root growth inhibition in response to flg22, but not to Pep1 (Fig. 4c; Fig. S4c). However, we cannot exclude the possibility that deregulated Ca^{2+} influx caused by $CNGC20^{L371F}$ activates *EDS1*- and *ICS1*-independent immunity pathways, thereby overriding the hyper-susceptibility of *eds1* or *sid2*.

The phenotypes discussed here emphasize the need for tight regulation of CNGC Ca^{2+} channel activity in order to limit host immunity and cell death in healthy, nonstimulated cells. In the absence of a biotic stress stimulus, calmodulin (CaM) interacts with the CaM-binding domains of Arabidopsis CNGC2 or CNGC4 and blocks the CNGC2-CNGC4 Ca^{2+} inward channel activity (Tian *et al.*, 2019). Upon PAMP or DAMP activation of PRRs, the channel is phosphorylated and activated by an RLCK signal transducer, BIK1 (Tian *et al.*, 2019). We find that CNGC20 also interacts with BIK1 and that BIK1 phosphorylates and stabilizes CNGC20 (Fig. 7). Collectively, these data are consistent with CNGC20 protein accumulation being positively regulated by BIK1 and negatively regulated by BAK1 (Yu *et al.*, 2019), perhaps to fine-tune plant cellular Ca^{2+} influx and immunity outputs.

The Arabidopsis *dnd1* autoimmune mutant lacking functional *CNGC2* exhibited different growth defects when grown alongside *cngc20-4* (Fig. 2d), suggesting that these two mutants impact cytosolic Ca^{2+} regulation in different ways. Indeed, SA was essential for *dnd1* enhanced disease resistance (Clough *et al.*, 2000) but not for *cngc20-4* autoimmunity (Fig. 4). Removing *ICS1*-generated SA and *EDS1* together in an *eds1 sid2* mutant, however, completely suppressed *cngc20-4* autoimmunity (Fig. 4), indicating that *cngc20-4* induced resistance is dependent on parallel *EDS1* and SA pathways (Cui *et al.*, 2017). Additionally, *dnd1* caused reduced Ca^{2+} influx and compromised ROS production upon flg22 treatment (Tian *et al.*, 2019), whereas *cngc20-4* increased cytosolic Ca^{2+} and enhanced an ROS burst in response to flg22 or Pep1 (Fig. 3b). It seems likely that increased cytosolic Ca^{2+} is responsible for the autoimmunity in *cngc20-4*. Cytosolic Ca^{2+} might enhance activation of calcium-dependent protein kinases (CPKs) such as CPK5, which directly phosphorylates and regulates RESPIRATORY BURST OXIDASE HOMOLOG D (RBOHD), a membrane localized NADPH oxidase for synthesizing ROS in PTI (Liang & Zhou, 2018). *CPK5* overexpression in Arabidopsis caused pathogen-induced cell death and enhanced resistance to powdery mildew fungi (Liu *et al.*, 2017). Cytosolic Ca^{2+} also activates a master transcription

Fig. 7 BIK1 interacts with and stabilizes CNGC20. (a) Split yellow fluorescent protein (YFP) assays reveal interaction between BIK1 and CNGC20 in *Nicotiana benthamiana* transient expression assays. Images were captured using a confocal microscope at 2 d after infiltration. Bars, 100 μm. (b–d) Co-immunoprecipitation (Co-IP) analysis of interactions between BIK1 and CNGC20 (b), $CNGC20^{L371F}$ (c), or the C-terminal domain of CNGC20 (CNGC20CT) (d) in transfected *Arabidopsis* Col protoplasts. Protoplasts were treated with 1 μM flg22 for 15 min before protein extraction in (b). Proteins in total extracts (labelled 'Input') and after IP with GFP-trap beads ('IP (YFP)') were detected on immunoblots using α-HA or α-GFP antibodies. (e) Glutathione-S-transferase (GST) pull-down analysis of interaction between BIK1 and CNGC20 C-terminal domain (CNGC20CT). Recombinant GST-CNGC20CT and His-BIK1 proteins purified from *Escherichiacoli* were used for GST pull-down assays. Interacting proteins were visualized with immunoblotting using α-His antibody. (f) BIK1 phosphorylates CNGC20CT *in vitro*. Recombinant GST-BIK1 and GST-CNGC20CT proteins purified from *E. coli* were used for *in vitro* phosphorylation assays. The phosphorylated GST-CNGC20CT was detected with α-phospho-threonine antibodies. (g) BIK1-HA enhances CNGC20-FLAG phosphorylation. CNGC20-FLAG was co-expressed with BIK1-HA, $BIK1^{D202A}$-HA or a control vector. After 15 min of flg22 treatment, CNGC20-FLAG was purified by immunoprecipitation with α-FLAG agarose. Total and phosphorylated CNGC20-FLAG were detected with α-FLAG and α-phospho-threonine antibodies. (h) Immunoblot analysis of CNGC20CT-FLAG and YFP-FLAG protein in a cell-free degradation assay. CNGC20CT-FLAG and YFP-FLAG were expressed and purified by immunoprecipitation with α-FLAG agarose from Arabidopsis protoplasts and incubated for the indicated times with total protein extracts from wild-type (WT) Col or *bik1* mutant leaves. FLAG-tagged proteins were detected with α-FLAG antibody. Ponceau staining of the blot shows equal protein loading. Experiments shown in (a–h) were repeated three times with consistent results.

factor CALMODULIN-BINDING PROTEIN60g (CBP60g), which functions in a partially redundant manner with its homolog SAR DEFICIENT1 (SARD1) to induce the expression of key regulators (including *ICS1*, *EDS1* and *PAD4*) in PTI, ETI and systemic immunity (Wang *et al.*, 2009; Wang *et al.*, 2011; Sun *et al.*, 2015).

Cngc20-4 caused a delay in flowering that was partially rescued by the combined loss of *EDS1* and *ICS1* (Fig. S4a), unlike many SA-related autoimmune plants, including *cpr22* (*CNGC11/12* chimera), which display an early flowering phenotype (Raskin, 1992; Fortuna *et al.*, 2015). Because delayed flowering was observed in *dnd1* (*cngc2*) and *dnd2* (*cngc4*) but not in *cngc3*, *11*, *12*, *19* or *20* loss-of-function mutants (Fortuna *et al.*, 2015), it is possible that *cngc20-4* reflects CNGC2 (and CNGC4) specific effects on flowering transition, linked to enhanced immunity.

Activation of NLR/NLRs is responsible for autoimmune phenotypes of many mutants (Gou & Hua, 2012; Zhang *et al.*, 2012; van Wersch *et al.*, 2016). The observed genetic redundancy between *ICS1*-generated SA and *EDS1* in *cngc20-4* autoimmunity (Fig. 4) is reminiscent of ETI triggered by Arabidopsis CNL RPS2 recognizing *Pst* delivered effector AvrRpt2, as RPS2-mediated restriction of bacterial growth was abolished in an *eds1 sid2* double mutant (Venugopal *et al.*, 2009; Cui *et al.*, 2017; Bhandari *et al.*, 2019). It was recently shown that cell death in *bak1 bkk1* requires a sub-group of 'helper' *NLRs (ADR1s)*, suggesting that *bak1 bkk1* cell death is a consequence of NLR activation (Wu *et al.*, 2020). These data and our findings raise the question for future work of whether perturbed CNGC Ca^{2+} channel activity and/or elevated cytosolic Ca^{2+} in *cngc20-4* induces certain NLRs to mobilize ETI responses.

Acknowledgements

We thank Prof. Zhi Qi for sharing *dnd1* seeds and protocols for visualizing extracellular Ca^{2+} distributions and Prof. Petra Dietrich for sharing *cngc19-1* and *cngc20-1* seeds. This work was funded by the National Natural Science Foundation of China (grant no. 31770277), Natural Science Foundation of Fujian Province (grant no. 2018J01609; HC, CZ), an Alexander von Humboldt Postdoctoral Fellowship (HC), Max-Planck Society (HC, JW, JEP) and Deutsche Forschungsgemeinschaft (German Research Foundation) SFB-1403–414786233 (JW, JEP).

Author contributions

HC and JEP designed and supervised the research; HC carried out the suppressor screening and characterization; CZ, YT, JW, YZ, ZZ, and RS performed the experiments; HS and KS analyzed genome-sequencing data; HC and JEP wrote the manuscript. CZ and YT contributed equally to this work.

ORCID

Haitao Cui https://orcid.org/0000-0002-6343-1014
Jane E. Parker https://orcid.org/0000-0002-4700-6480
Junli Wang https://orcid.org/0000-0001-8825-3894

References

Adlung N, Prochaska H, Thieme S, Banik A, Bluher D, John P, Nagel O, Schulze S, Gantner J, Delker C *et al.* 2016. Non-host resistance induced by the *Xanthomonas* effector XopQ is widespread within the genus *Nicotiana* and functionally depends on EDS1. *Frontiers in Plant Science* **7**: 1796.

Atkinson MM, Keppler LD, Orlandi EW, Baker CJ, Mischke CF. 1990. Involvement of plasma membrane calcium influx in bacterial induction of the k/h and hypersensitive responses in tobacco. *Plant Physiology* **92**: 215–221.

Bartsch M, Gobbato E, Bednarek P, Debey S, Schultze JL, Bautor J, Parker JE. 2006. Salicylic acid-independent ENHANCED DISEASE SUSCEPTIBILITY1 signaling in *Arabidopsis* immunity and cell death is regulated by the monooxygenase *FMO1* and the Nudix hydrolase *NUDT7*. *The Plant Cell* **18**: 1038–1051.

Bhandari DD, Lapin D, Kracher B, von Born P, Bautor J, Niefind K, Parker JE. 2019. An EDS1 heterodimer signalling surface enforces timely reprogramming of immunity genes in *Arabidopsis*. *Nature Communications* **10**: 772.

Blume B, Nurnberger T, Nass N, Scheel D. 2000. Receptor-mediated increase in cytoplasmic free calcium required for activation of pathogen defense in parsley. *The Plant Cell* **12**: 1425–1440.

Boudsocq M, Willmann MR, McCormack M, Lee H, Shan L, He P, Bush J, Cheng SH, Sheen J. 2010. Differential innate immune signalling via Ca^{2+} sensor protein kinases. *Nature* **464**: 418–422.

Chin K, DeFalco TA, Moeder W, Yoshioka K. 2013. The Arabidopsis cyclic nucleotide-gated ion channels AtCNGC2 and AtCNGC4 work in the same signaling pathway to regulate pathogen defense and floral transition. *Plant Physiology* **163**: 611–624.

Clough SJ, Fengler KA, Yu IC, Lippok B, Smith RK Jr, Bent AF. 2000. The *Arabidopsis dnd1* "defense, no death" gene encodes a mutated cyclic nucleotide-gated ion channel. *Proceedings of the National Academy of Sciences, USA* **97**: 9323–9328.

Cui H, Gobbato E, Kracher B, Qiu J, Bautor J, Parker JE. 2017. A core function of EDS1 with PAD4 is to protect the salicylic acid defense sector in Arabidopsis immunity. *New Phytologist* **213**: 1802–1817.

Cui H, Qiu J, Zhou Y, Bhandari DD, Zhao C, Bautor J, Parker JE. 2018. Antagonism of transcription factor MYC2 by EDS1/PAD4 complexes bolsters salicylic acid defense in Arabidopsis effector-triggered immunity. *Molecular Plant* **11**: 1053–1066.

Cui H, Tsuda K, Parker JE. 2015. Effector-triggered immunity: from pathogen perception to robust defense. *Annual Review of Plant Biology* **66**: 487–511.

Engler C, Youles M, Gruetzner R, Ehnert TM, Werner S, Jones JD, Patron NJ, Marillonnet S. 2014. A golden gate modular cloning toolbox for plants. *ACS Synthetic Biology* **3**: 839–843.

Feys BJ, Moisan LJ, Newman MA, Parker JE. 2001. Direct interaction between the *Arabidopsis* disease resistance signaling proteins, EDS1 and PAD4. *EMBO Journal* **20**: 5400–5411.

Feys BJ, Wiermer M, Bhat RA, Moisan LJ, Medina-Escobar N, Neu C, Cabral A, Parker JE. 2005. *Arabidopsis* SENESCENCE-ASSOCIATED GENE101 stabilizes and signals within an ENHANCED DISEASE SUSCEPTIBILITY1 complex in plant innate immunity. *The Plant Cell* **17**: 2601–2613.

Fortuna A, Lee J, Ung H, Chin K, Moeder W, Yoshioka K. 2015. Crossroads of stress responses, development and flowering regulation–the multiple roles of Cyclic Nucleotide Gated Ion Channel 2. *Plant Signaling Behaviour* **10**: e989758.

Fu ZQ, Dong X. 2013. Systemic acquired resistance: turning local infection into global defense. *Annual Review of Plant Biology* **64**: 839–863.

Gantner J, Ordon J, Kretschmer C, Guerois R, Stuttmann J. 2019. An EDS1-SAG101 complex is essential for TNL-mediated immunity in *Nicotiana benthamiana*. *The Plant Cell* **31**: 2456–2474.

Gao X, Ruan X, Sun Y, Wang X, Feng B. 2018. BAKing up to survive a battle: functional dynamics of BAK1 in plant programmed cell death. *Front Plant Sci* **9**: 1913.

Gilliham M, Dayod M, Hocking BJ, Xu B, Conn SJ, Kaiser BN, Leigh RA, Tyerman SD. 2011. Calcium delivery and storage in plant leaves: exploring the link with water flow. *Journal of Experimental Botany* **62**: 2233–2250.

Gou M, Hua J. 2012. Complex regulation of an R gene *SNC1* revealed by autoimmune mutants. *Plant Signaling & Behavior* **7**: 213–216.

Grant M, Brown I, Adams S, Knight M, Ainslie A, Mansfield J. 2000. The *RPM1* plant disease resistance gene facilitates a rapid and sustained increase in cytosolic calcium that is necessary for the oxidative burst and hypersensitive cell death. *The Plant Journal* **23**: 441–450.

He K, Gou X, Yuan T, Lin H, Asami T, Yoshida S, Russell SD, Li J. 2007. BAK1 and BKK1 regulate brassinosteroid-dependent growth and brassinosteroid-independent cell-death pathways. *Current Biology* **17**: 1109–1115.

Heidrich K, Wirthmueller L, Tasset C, Pouzet C, Deslandes L, Parker JE. 2011. *Arabidopsis* EDS1 connects pathogen effector recognition to cell compartment-specific immune responses. *Science* **334**: 1401–1404.

Horsefield S, Burdett H, Zhang X, Manik MK, Shi Y, Chen J, Qi T, Gilley J, Lai JS, Rank MX *et al.* 2019. NAD^+ cleavage activity by animal and plant TIR domains in cell death pathways. *Science* **365**: 793–799.

Jones JD, Dangl JL. 2006. The plant immune system. *Nature* **444**: 323–329.

Jubic LM, Saile S, Furzer OJ, El Kasmi F, Dangl JL. 2019. Help wanted: helper NLRs and plant immune responses. *Current Opinion in Plant Biology* **50**: 82–94.

Jurkowski GI, Smith RK Jr, Yu IC, Ham JH, Sharma SB, Klessig DF, Fengler KA, Bent AF. 2004. Arabidopsis *DND2*, a second cyclic nucleotide-gated ion channel gene for which mutation causes the "defense, no death" phenotype. *Molecular Plant-Microbe Interactions* **17**: 511–520.

Kadota Y, Liebrand TWH, Goto Y, Sklenar J, Derbyshire P, Menke FLH, Torres MA, Molina A, Zipfel C, Coaker G *et al.* 2019. Quantitative phosphoproteomic analysis reveals common regulatory mechanisms between effector- and PAMP-triggered immunity in plants. *New Phytologist* **221**: 2160–2175.

Kemmerling B, Schwedt A, Rodriguez P, Mazzotta S, Frank M, Qamar SA, Mengiste T, Betsuyaku S, Parker JE, Mussig C *et al.* 2007. The BRI1-associated kinase 1, BAK1, has a brassinolide-independent role in plant cell-death control. *Current Biology* **17**: 1116–1122.

Kobayashi M, Ohura I, Kawakita K, Yokota N, Fujiwara M, Shimamoto K, Doke N, Yoshioka H. 2007. Calcium-dependent protein kinases regulate the production of reactive oxygen species by potato NADPH oxidase. *The Plant Cell* **19**: 1065–1080.

Kugler A, Kohler B, Palme K, Wolff P, Dietrich P. 2009. Salt-dependent regulation of a CNG channel subfamily in Arabidopsis. *BMC Plant Biology* **9**: 140.

Laluk K, Luo H, Chai M, Dhawan R, Lai Z, Mengiste T. 2011. Biochemical and genetic requirements for function of the immune response regulator *BOTRYTIS-INDUCED KINASE1* in plant growth, ethylene signaling, and PAMP-triggered immunity in Arabidopsis. *The Plant Cell* **23**: 2831–2849.

Lapin D, Bhandari DD, Parker JE. 2020. Origins and immunity networking functions of EDS1 family proteins. *Annual review of Phytopathology* **58**: 253–276.

Lapin D, Kovacova V, Sun X, Dongus JA, Bhandari D, von Born P, Bautor J, Guarneri N, Rzemieniewski J, Stuttmann J *et al.* 2019. A coevolved EDS1-SAG101-NRG1 module mediates cell death signaling by TIR-domain immune receptors. *The Plant Cell* **31**: 2430–2455.

Lee CH, MacKinnon R. 2017. Structures of the human HCN1 hyperpolarization-activated channel. *Cell* **168**: 111–120.

Leng Q, Mercier RW, Hua BG, Fromm H, Berkowitz GA. 2002. Electrophysiological analysis of cloned cyclic nucleotide-gated ion channels. *Plant Physiology* **128**: 400–410.

Li L, Li M, Yu L, Zhou Z, Liang X, Liu Z, Cai G, Gao L, Zhang X, Wang Y *et al.* 2014. The FLS2-associated kinase BIK1 directly phosphorylates the NADPH oxidase RbohD to control plant immunity. *Cell Host & Microbe* **15**: 329–338.

Liang X, Zhou JM. 2018. Receptor-like cytoplasmic kinases: central players in plant receptor kinase-mediated signaling. *Annual Review of Plant Biology* **69**: 267–299.

Liu N, Hake K, Wang W, Zhao T, Romeis T, Tang D. 2017. CALCIUM-DEPENDENT PROTEIN KINASE5 associates with the truncated NLR protein TIR-NBS2 to contribute to *exo70B1*-mediated immunity. *The Plant Cell* **29**: 746–759.

Liu Z, Wu Y, Yang F, Zhang Y, Chen S, Xie Q, Tian X, Zhou JM. 2013. BIK1 interacts with PEPRs to mediate ethylene-induced immunity. *Proceedings of the National Academy of Sciences, USA* **110**: 6205–6210.

Ma S, Lapin D, Liu L, Sun Y, Song W, Zhang X, Logemann E, Yu D, Wang J, Jirschitzka J *et al.* 2020. Direct pathogen-induced assembly of an NLR immune receptor complex to form a holoenzyme. *Science* **370**: eabd9993.

Ma Y, Guo H, Hu L, Martinez PP, Moschou PN, Cevik V, Ding P, Duxbury Z, Sarris PF, Jones JDG. 2018. Distinct modes of derepression of an Arabidopsis immune receptor complex by two different bacterial effectors. *Proceedings of the National Academy of Sciences, USA* **115**: 10218–10227.

Ma Y, Walker RK, Zhao Y, Berkowitz GA. 2012. Linking ligand perception by PEPR pattern recognition receptors to cytosolic Ca^{2+} elevation and downstream immune signaling in plants. *Proceedings of the National Academy of Sciences, USA* **109**: 19852–19857.

Ma Y, Zhao Y, Walker RK, Berkowitz GA. 2013. Molecular steps in the immune signaling pathway evoked by plant elicitor peptides: Ca^{2+}-dependent protein kinases, nitric oxide, and reactive oxygen species are downstream from the early Ca^{2+} signal. *Plant Physiology* **163**: 1459–1471.

Martin R, Qi T, Zhang H, Liu F, King M, Toth C, Nogales E, Staskawicz BJ. 2020. Structure of the activated ROQ1 resistosome directly recognizing the pathogen effector XopQ. *Science* **370**: eabd9993.

Mäser P, Thomine S, Schroeder JI, Ward JM, Hirschi K, Sze H, Talke IN, Amtmann A, Maathuis FJM, Sanders D *et al.* 2001. Phylogenetic relationships within cation transporter families of Arabidopsis. *Plant Physiology* **126**: 1646–1667.

Meena MK, Prajapati R, Krishna D, Divakaran K, Pandey Y, Reichelt M, Mathew MK, Boland W, Mithofer A, Vadassery J. 2019. The Ca^{2+} channel *CNGC19* regulates Arabidopsis defense against *Spodoptera* herbivory. *The Plant Cell* **31**: 1539–1562.

Moeder W, Phan V, Yoshioka K. 2019. Ca^{2+} to the rescue – Ca^{2+} channels and signaling in plant immunity. *Plant Science* **279**: 19–26.

Navarro L, Bari R, Achard P, Lison P, Nemri A, Harberd NP, Jones JD. 2008. DELLAs control plant immune responses by modulating the balance of jasmonic acid and salicylic acid signaling. *Current Biology* **18**: 650–655.

Ngou BPM, Ahn H-K, Ding P, Jones JD. 2020. Mutual potentiation of plant immunity by cell-surface and intracellular receptors. *bioRxiv*: doi: 10.1101/2020.04.10.034173.

Ossowski S, Schneeberger K, Clark RM, Lanz C, Warthmann N, Weigel D. 2008. Sequencing of natural strains of Arabidopsis thaliana with short reads. *Genome Research* **18**: 2024–2033.

Pan Y, Chai X, Gao Q, Zhou L, Zhang S, Li L, Luan S. 2019. Dynamic interactions of plant CNGC subunits and calmodulins drive oscillatory Ca^{2+} channel activities. *Developmental Cell* **48**: 710–725.e5.

Qi T, Seong K, Thomazella DPT, Kim JR, Pham J, Seo E, Cho MJ, Schultink A, Staskawicz BJ. 2018. *NRG1* functions downstream of *EDS1* to regulate TIR-NLR-mediated plant immunity in *Nicotiana benthamiana*. *Proceedings of the National Academy of Sciences, USA* **115**: E10979–E10987.

Qi Z, Verma R, Gehring C, Yamaguchi Y, Zhao Y, Ryan CA, Berkowitz GA. 2010. Ca^{2+} signaling by plant *Arabidopsis thaliana* Pep peptides depends on AtPepR1, a receptor with guanylyl cyclase activity, and cGMP-activated Ca^{2+} channels. *Proceedings of the National Academy of Sciences, USA* **107**: 21193–21198.

Ranf S, Eschen-Lippold L, Pecher P, Lee J, Scheel D. 2011. Interplay between calcium signalling and early signalling elements during defence responses to microbe- or damage-associated molecular patterns. *The Plant Journal* **68**: 100–113.

Raskin I. 1992. Role of salicylic acid in plants. *Annual Review of Plant Physiology and Plant Molecular Biology* **43**: 439–463.

Rietz S, Stamm A, Malonek S, Wagner S, Becker D, Medina-Escobar N, Vlot AC, Feys BJ, Niefind K, Parker JE. 2011. Different roles of Enhanced Disease Susceptibility1 (EDS1) bound to and dissociated from Phytoalexin Deficient4 (PAD4) in Arabidopsis immunity. *New Phytologist* **191**: 107–119.

Saucet SB, Ma Y, Sarris PF, Furzer OJ, Sohn KH, Jones JD. 2015. Two linked pairs of *Arabidopsis TNL* resistance genes independently confer recognition of bacterial effector AvrRps4. *Nature Communications* **6**: 6338.

Schneeberger K, Hagmann J, Ossowski S, Warthmann N, Gesing S, Kohlbacher O, Weigel D. 2009. Simultaneous alignment of short reads against multiple genomes. *Genome Biology* **10**: R98.

Seybold H, Trempel F, Ranf S, Scheel D, Romeis T, Lee J. 2014. Ca^{2+} signalling in plant immune response: from pattern recognition receptors to Ca^{2+} decoding mechanisms. *New Phytologist* **204**: 782–790.

Sheard LB, Tan X, Mao H, Withers J, Ben-Nissan G, Hinds TR, Kobayashi Y, Hsu FF, Sharon M, Browse J *et al.* 2010. Jasmonate perception by inositol-phosphate-potentiated COI1-JAZ co-receptor. *Nature* **468**: 400–405.

Suarez-Rodriguez MC, Adams-Phillips L, Liu Y, Wang H, Su SH, Jester PJ, Zhang S, Bent AF, Krysan PJ. 2007. MEKK1 is required for flg22-induced MPK4 activation in Arabidopsis plants. *Plant Physiology* **143**: 661–669.

Sun H, Schneeberger K. 2015. SHOREmap v3.0: fast and accurate identification of causal mutations from forward genetic screens. *Methods in Molecular Biology* **1284**: 381–395.

Sun T, Zhang Y, Li Y, Zhang Q, Ding Y, Zhang Y. 2015. ChIP-seq reveals broad roles of SARD1 and CBP60g in regulating plant immunity. *Nature Communications* **6**: 10159.

Tian W, Hou C, Ren Z, Wang C, Zhao F, Dahlbeck D, Hu S, Zhang L, Niu Q, Li L *et al.* 2019. A calmodulin-gated calcium channel links pathogen patterns to plant immunity. *Nature* **572**: 131–135.

Toyota M, Spencer D, Sawai-Toyota S, Jiaqi W, Zhang T, Koo AJ, Howe GA, Gilroy S. 2018. Glutamate triggers long-distance, calcium-based plant defense signaling. *Science* **361**: 1112–1115.

Venugopal SC, Jeong RD, Mandal MK, Zhu S, Chandra-Shekara AC, Xia Y, Hersh M, Stromberg AJ, Navarre D, Kachroo A *et al.* 2009. Enhanced disease susceptibility 1 and salicylic acid act redundantly to regulate resistance gene-mediated signaling. *PLoS Genetics* **5**: e1000545.

Wagner S, Stuttmann J, Rietz S, Guerois R, Brunstein E, Bautor J, Niefind K, Parker JE. 2013. Structural basis for signaling by exclusive EDS1 heteromeric complexes with SAG101 or PAD4 in plant innate immunity. *Cell Host & Microbe* **14**: 619–630.

Wan L, Essuman K, Anderson RG, Sasaki Y, Monteiro F, Chung EH, Osborne Nishimura E, DiAntonio A, Milbrandt J, Dangl JL *et al.* 2019. TIR domains of plant immune receptors are NAD^+-cleaving enzymes that promote cell death. *Science* **365**: 799–803.

Wang J, Hu M, Wang J, Qi J, Han Z, Wang G, Qi Y, Wang HW, Zhou JM, Chai J. 2019a. Reconstitution and structure of a plant NLR resistosome conferring immunity. *Science* **364**.

Wang J, Liu X, Zhang A, Ren Y, Wu F, Wang G, Xu Y, Lei C, Zhu S, Pan T *et al.* 2019b. A cyclic nucleotide-gated channel mediates cytoplasmic calcium elevation and disease resistance in rice. *Cell Research* **29**: 820–831.

Wang J, Wang J, Hu M, Wu S, Qi J, Wang G, Han Z, Qi Y, Gao N, Wang HW *et al.* 2019c. Ligand-triggered allosteric ADP release primes a plant NLR complex. *Science* **364**.

Wang L, Tsuda K, Sato M, Cohen JD, Katagiri F, Glazebrook J. 2009. Arabidopsis CaM binding protein CBP60g contributes to MAMP-induced SA accumulation and is involved in disease resistance against *Pseudomonas syringae*. *PLoS Path* **5**: e1000301.

Wang L, Tsuda K, Truman W, Sato M, le Nguyen V, Katagiri F, Glazebrook J. 2011. CBP60g and SARD1 play partially redundant critical roles in salicylic acid signaling. *The Plant Journal* **67**: 1029–1041.

Wang W, Feng B, Zhou JM, Tang D. 2020. Plant immune signaling: Advancing on two frontiers. *Journal of Integrative Plant Biology* **62**: 2–24.

Wang Y, Kang Y, Ma C, Miao R, Wu C, Long Y, Ge T, Wu Z, Hou X, Zhang J *et al.* 2017. CNGC2 Is a Ca^{2+} influx channel that prevents accumulation of apoplastic Ca^{2+} in the leaf. *Plant Physiology* **173**: 1342–1354.

van Wersch R, Li X, Zhang Y. 2016. Mighty dwarfs: Arabidopsis autoimmune mutants and their usages in genetic dissection of plant immunity. *Frontiers Plant Science* **7**: 1717.

White PJ. 2001. The pathways of calcium movement to the xylem. *Journal of Experimental Botany* **52**: 891–899.

Wildermuth MC, Dewdney J, Wu G, Ausubel FM. 2001. Isochorismate synthase is required to synthesize salicylic acid for plant defence. *Nature* **414**: 562–565.

Wu Y, Gao Y, Zhan Y, Kui H, Liu H, Yan L, Kemmerling B, Zhou JM, He K, Li J. 2020. Loss of the common immune coreceptor BAK1 leads to NLR-dependent cell death. *Proceedings of the National Academy of Sciences, USA* **117**: 27044–27053.

Xin XF, He SY. 2013. *Pseudomonas syringae* pv. *tomato* DC3000: a model pathogen for probing disease susceptibility and hormone signaling in plants. *Annual Review of Phytopathology* **51**: 473–498.

Yamada K, Yamashita-Yamada M, Hirase T, Fujiwara T, Tsuda K, Hiruma K, Saijo Y. 2016. Danger peptide receptor signaling in plants ensures basal immunity upon pathogen-induced depletion of BAK1. *Embo Journal* **35**: 46–61.

Yi SY, Shirasu K, Moon JS, Lee SG, Kwon SY. 2014. The activated SA and JA signaling pathways have an influence on flg22-triggered oxidative burst and callose deposition. *PLoS ONE* **9**: e88951.

Yoshioka K, Moeder W, Kang HG, Kachroo P, Masmoudi K, Berkowitz G, Klessig DF. 2006. The chimeric *Arabidopsis* CYCLIC NUCLEOTIDE-GATED ION CHANNEL11/12 activates multiple pathogen resistance responses. *The Plant Cell* **18**: 747–763.

Yu IC, Parker J, Bent AF. 1998. Gene-for-gene disease resistance without the hypersensitive response in *Arabidopsis dnd1* mutant. *Proceedings of the National Academy of Sciences, USA* **95**: 7819–7824.

Yu X, Xu G, Li B, de Souza VL, Liu H, Moeder W, Chen S, de Oliveira MVV, Ariadina de Souza S, Shao W *et al.* 2019. The receptor kinases BAK1/SERK4 regulate Ca^{2+} channel-mediated cellular homeostasis for cell death containment. *Current Biology* **29**: 3778–3790.

Yuan M, Jiang Z, Bi G, Nomura K, Liu M, He SY, Zhou J-M, Xin X-F. 2020. Pattern-recognition receptors are required for NLR-mediated plant immunity. https://doi.org/10.1101/2020.04.10.031294

Zelman AK, Dawe A, Gehring C, Berkowitz GA. 2012. Evolutionary and structural perspectives of plant cyclic nucleotide-gated cation channels. *Frontiers in Plant Science* **3**: 95.

Zhang Y, Li X. 2019. Salicylic acid: biosynthesis, perception, and contributions to plant immunity. *Current Opinion in Plant Biology* **50**: 29–36.

Zhang Z, Wu Y, Gao M, Zhang J, Kong Q, Liu Y, Ba H, Zhou J, Zhang Y. 2012. Disruption of PAMP-induced MAP kinase cascade by a *Pseudomonas syringae* effector activates plant immunity mediated by the NB-LRR protein SUMM2. *Cell Host & Microbe* **11**: 253–263.

Supporting Information

Additional Supporting Information may be found online in the Supporting Information section at the end of the article.

Fig. S1 Sequence alignment of CYCLIC NUCLEOTIDE-GATED CHANNEL (CNGC) family proteins and phenotypes of *cngc20* and *cngc19* mutants.

Fig. S2 Transiently expressed $CNGC20^{L371F}$ enhances resistance to *Xanthomonas campestris* pv *vesicatoria* bacteria in an *Nicotiana benthamiana eds1a* mutant.

Fig. S3 Flg22-induced immune responses in *cngc20* and *cngc19* mutants.

Fig. S4 Flowering and Pep1-induced growth inhibition in *eds1-2 sid2-1 cngc20-4*.

Fig. S5 Predicated CNGC20 tetrameric protein complex structure.

Fig. S6 A model for *cngc20-4*-mediated enhanced immunity.

Table S1 Oligonucleotides used in this work.

Please note: Wiley Blackwell are not responsible for the content or functionality of any Supporting Information supplied by the authors. Any queries (other than missing material) should be directed to the *New Phytologist* Central Office.